國立成功大學

太空與電漿科學研究所

碩士論文

National Cheng Kung University

Institute of Space and Plasma Sciences

Master Thesis

EUV光源中角向捏縮磁場之開發

Development of the magnetic field in a theta pinch in the EUV light source

研究生 (Author)：杜承翰 Cheng-Han Du

指導老師 (Advisor)：張博宇博士 Dr. Po-Yu Chang

中華民國一百一十一年七月 July, 2022

國立成功大學

碩士論文

EUV光源中角向捏縮磁場之開發

Development of the magnetic field in a theta pinch in the EUV light source

研究生：杜承翰

本論文業經審查及口試合格特此證明

論文考試委員：張博宇

劉耀豐

曲宏宇

指導教授：張博宇

單位主管：電漿所所長河森榮一郎

（單位主管是否簽章授權由各院、系（所、學位學程）自訂）

中 華 民 國 111 年 7 月 21 日

摘要

極紫外光微影是半導體製程中最先進的技術之一，我們將透過角向捏縮的方式來壓縮加熱電漿，使電漿的溫度到達約 30 eV，因而輻射出極紫外光。在本論文中，我們使用荷姆霍茲線圈去產生角向捏縮所需的磁場。爲了驅動荷姆霍茲線圈，我們使用實驗室中的脈衝功率系統，這系統能夠提供峰值達 100 ∼ 200 kA、上升時間約爲 1.6 μs的大電流。荷姆霍茲線圈是由不鏽鋼所製成，線圈的截面積爲一矩形，厚度爲 2.5 mm，線圈的內半徑和外半徑分別是 5 mm 和 15 mm。它的結構堅固，不會因大電流而損壞。根據線圈磁場的公式，理想的荷姆霍茲線圈能在中心處產生 4.6∼11.6 T 的磁場。在模擬中，考量電流均勻分布在線圈的截面積中，則荷姆霍茲線圈在中心處產生10.1 T的磁場。最後，我們透過放電測試量測磁場。在荷姆霍茲線圈放電測試中，我們利用半徑爲 2.5 mm 的單匝線圈所製的B點探針(B-dot probe)，來測量荷姆霍茲線圈產生的磁場。首先，B點探針先透過自製的螺線管產生已知磁場進行校正。從實驗中，我們得到B點探針校正因子是41500±300(T/V·sec)。然後，我們使用RC積分器將B點探針的感應電壓積分得到待測的磁場。最後，我們量測得到荷姆霍茲線圈在中心點位置的磁場峰值爲11.4±1.0 T。

關鍵字:極紫外光、角向捏縮、荷姆霍茲線圈、脈衝功率系統、B點探針

Abstract

Extreme ultraviolet (EUV) lithography is one of the most advanced technologies in semiconductor fabrication. We would like to heat the plasma using a theta pinch via compression heating. When the temperature of the plasma reaches about 30 eV, the plasma radiates EUV light. In this thesis, we used a Helmholtz coil to generate the magnetic field required for the theta pinch. In order to drive the theta pinch, we used a pulsed-power system in the laboratory, which can provide a high current with a peak of $100 \sim 200$ kA and a rise time of $\sim 1.6\,\mu$s. The Helmholtz coil is made of stainless steel. The cross section of the coil is rectangular with 2.5 mm in thickness. The inner and the outer radius of the coil are 5 mm and 15 mm, respectively. The structure of the coil is strong and is not damaged by the high current. According to the theoretical formula , the ideal Helmholtz coil can generate a magnetic field in the range of 4.6 to 11.6 T at the center. In the simulation, current is uniformly distributed in the cross section, the ideal Helmholtz coil produced a magnetic field of 10.1 T at the center. Finally, we experimentally measured the magnetic field through discharge test. In the Helmholtz coil discharge tests, we used a B-dot probe to measure the magnetic field generated by the Helmholtz coil. The B-dot probe was a single-turn coil with a radius of 2.5 mm. It was first calibrated by an known magnetic field generated by a self-made solenoid. In experiments, we obtained that the calibration ratio C_{calib} of the B-dot probe was 41500±300 (T/V·sec). In addition, we used the RC integrator to integrate the induced voltage of the B-dot probe to obtain the magnetic field. Finally, the measured peak magnetic field generated by the Helmholtz coil at the center was 11.4±1.0 T.

Keywords: extreme ultraviolet light, theta pinch, Helmholtz coil, pulsed-power system, B-dot probe

致謝

兩年前，來到了成大電漿所，加入了張博宇教授的PPL實驗室。當初還擔心實驗室的生活會不適應，幸好實驗室的氣氛很好，不管是學長、同儕，還是學弟都能和睦的相處，在遇到問題或困難的時候，都能同心協力、互相幫助，使得實驗室裡系統的建置日漸完善。老師總是耐心提醒我們實驗上的細節，每當遇到問題時，老師不會馬上給我答案，而是用引導的方式去讓我思考解決問題的方法。不管是做實驗，還是寫報告，老師都會適時的告訴我要改進的地方，使我更有條理地完成一件事情。我們實驗室的實驗計畫都是要由好幾屆學生的接續完成的，每一位學長姐和學弟都在實驗中扮演重要的角色，而我也是其中一員，負責我們計畫中的一個環節。然而計畫尚未完成，期許未來的學弟能夠將實驗的目標達成，將實驗室發揚光大。感謝我爸媽，幫我繳學雜費，讓我不用背學貸，安安心心讀完這兩年的碩士。最後，感謝老師、實驗室的夥伴、系辦人員，還有教過我的教授，這兩年我學到了許多。再見了成大電漿所、PPL實驗室。

Contents

List of Figures

List of Tables

1 Introduction

We are developing a new way of generating the Extreme ultraviolet (EUV) light sources using discharge-produced plasma (DPP). We would like to compress a plasma plume using a theta pinch. Therefore, the plasma plume reaches a temperature of ∼30 eV and radiates EUV light. In this chapter, the EUV lithography in semiconductor fabrication will be introduced in section 1.1. In section 1.2, the information of the conventional EUV source will be introduced. The typical theta-pinch experiment will be introduced in section 1.3. The pulsed-power system will be introduced in section 1.4. Then, the section 1.5 is about the information of Helmholtz coil. Finally, our proposed EUV light source and the goal of the thesis will be introduced in section 1.6.

1.1 Extreme ultraviolet (EUV) lithography

For the past decades, the rapid development of semiconductor fabrication technology has greatly changed our lives. Semiconductor fabrication is a complex and time-consuming process as shown in Figure 1.

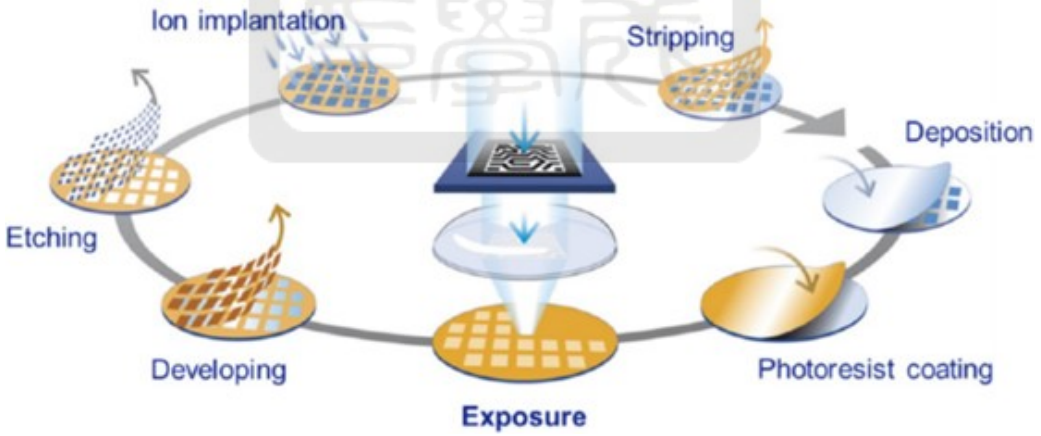

Figure 1: The process of semiconductor fabrication [1].

The optical lithography fabrication is one of the steps. The technique of lithography fabrication is to transfer the designed pattern from the photomasks or reticles to the photoresist on the wafer surface [1]. Then, the designed circuit pattern can be made on the wafer surface via etching and ion implantation. Therefore, the lithography fabrication is one of the important technologies in the semiconductor process.

Moore's law states that the number of transistors in a dense integrated circuit (IC) doubles about every two years [2]. Many scientists and engineers continue to push the physical limits of the component size, taking semiconductors from the 250-nm node in 1997 to the 7-nm node in 2018. In theory, as long as the size of the photomasks is reduced, the size of the integrated circuit can continue to be reduced. But, when the size is less than a half of the wavelength of light, the light will diffract as shown in Figure 2 [3]. The problem makes it difficult to shrink the size of the semiconductor. In order to make the smaller semiconductor components, light with the shorter wavelength is needed. Nowadays, the extreme ultraviolet (EUV) light with a center wavelength of 13.5 nm is used.

Figure 2: The optical diffraction makes semiconductors shrink more difficult [3].

1.2 The conventional EUV source

The leading technology of generating EUV light is to heat the plasma to reach ∼30 eV. At this temperature, the plasma emits light in the range from EUV to infrared from electron transitions between the different energy levels or bremsstrahlung radiations from free electrons. Laser-produced plasma (LPP) and discharge-produced plasma (DPP) are the two ways for generating high-power EUV radiation at 13.5 nm. Nowadays, LPP is widely used by the electronics industry, e.g., Taiwan Semiconductor Manufacturing Company (TSMC). In LPP, the target material (Tin) heated by a high intensity laser pulse becomes the high-temperature plasma and emits the 13.5 nm EUV light. In semiconductor market, ASML is a well-known semiconductor equipment supplier, mainly providing the EUV exposure machines to customers. The EUV lithography system provides by ASML is shown in Figure 3 [4].

Figure 3: The EUV exposure machines of ASML [4].

In DPP, hot plasma can be created from the low-temperature plasma through the magnetic compress, called the "pinch effect." Plasma is compressed with the magnetic field generated from the current since the charged particles in the plasma are moved by the Lorentz force. If it is compressed fast enough, the low-temperature plasma can be heated adiabatically. Figure 4 shows the two typical compression mechanism in DPP. The first one is called the "z-pinch," and the second one is called the "theta pinch." In a z-pinch, the current flows through the surface of a cylindrical plasma in the z-direction. An azimuthal magnetic field is generated at the same time. The Lorentz force on each current path is in the radial direction pointing toward the center of the cylindrical plasma. Therefore, the plasma is compressed to the center and heated. Because the current is in the z direction, the mechanism is called the z-pinch. On the other hand, in a theta pinch, the time-varying current flows through a coil in the azimuthal direction. A magnetic field in the z direction is generated by the current and varies with time. Then, an azimuthal current I_{plasma} in the plasma, which is located at the center of the coil, is induced. The Lorentz force that generates from the plasma current I_{plasma} interacting with the magnetic field is in the radial direction toward the center of the plasma. Finally, the plasma is also compressed. Since the current is in the azimuthal direction, the mechanism is called the theta pinch.

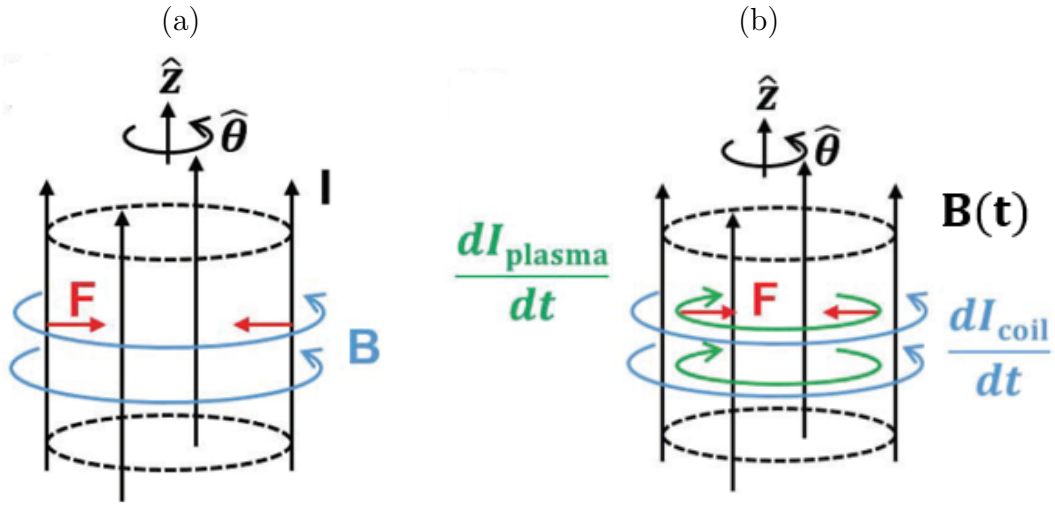

Figure 4: (a) z-pinch. (b) theta pinch.

1.3 The typical theta-pinch experiment

The schematic diagram of the typical theta-pinch experiment is illustrated in Figure 5 [5]. The plasma fills in an insulting discharge tube (e.g., made of quartz or Pyrex), which is surrounded by a single turn coil connected to a large capacitor bank. The gas is pre-ionized in the tube before the switch of the capacitor bank is turned on. When the capacitor discharges, the current I_C flows through the coil and produces a magnetic field B_C in the tube. The plasma is diamagnetic and a magnetic field B_P in the direction opposite to the magnetic field B_C, which is applied on it, is generated. Based on Faraday's law of induction, the magnetic field B_C induces an azimuthal current I_P in the pre-ionized plasma. The difference of the external and the internal magnetic field produces a magnetic pressure difference which pushes the plasma inward radially. It makes the plasma start to adiabatically compress inward radially. When the external magnetic pressure is balanced by the plasma pressure, the compression stops and it is called stagnation. The theta-pinch experiment of our proposed EUV light source is similar to the typical theta-pinch experiment and will be introduced in section 1.6.

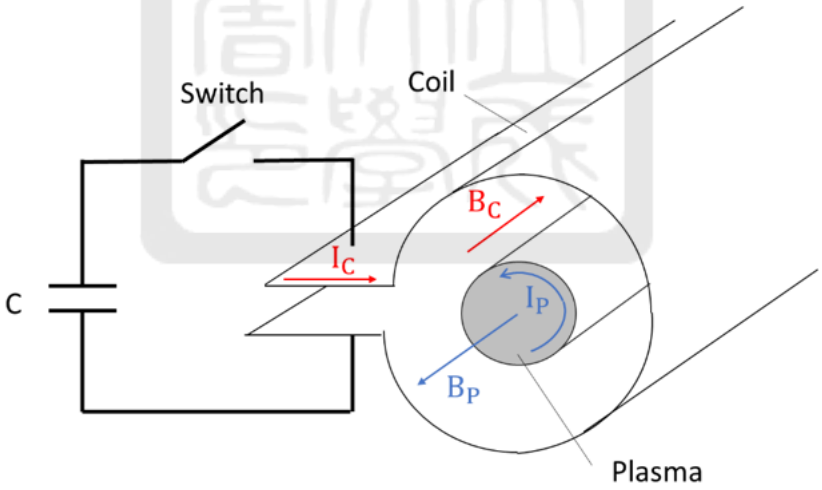

Figure 5: The schematic of theta-pinch experiment [5].

1.4 The pulsed-power system

The theta-pinch will be implemented on the pulsed-power system we built. In the theta-pinch, a Helmholtz coil driven by the pulsed-power system is used to provide the pulsed magnetic field to compress the plasma plume. The pulsed-power system as shown in Figure 6 is the main platform for conducting experiments in our laboratory [6]. The pulsed-power system is a device that can be used to study phenomena using high power, high voltage and high current. The device stores large energy in the capacitor bank and releases the energy to the load in a short period of time. The pulsed-power system is widely used. It is used to study laboratory astrophysics, plasma physics in high-energy-density-plasma (HEDP) regime, nuclear fusion energy, and the soft x ray/ EUV light source. At present, we study HEDP with two different pinches. One is the z-pinch, and the other one is the theta-pinch. Both pinches are driven by the pulsed-power system. Therefore, the high-temperature and high-density plasma can be generated or heated through two kinds of pinches. Finally, the detail information of the pulsed-power system will be given in Chapter 2.

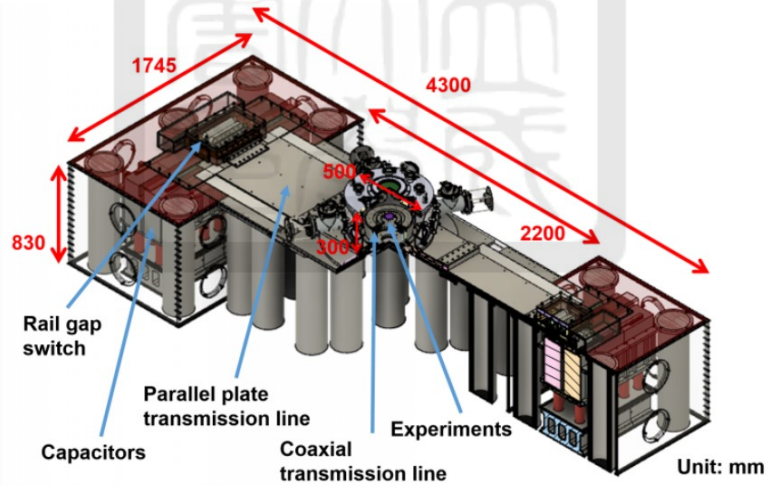

Figure 6: The CAD drawing of the pulsed-power system [6].

1.5 Helmholtz coil

Helmholtz coil is a device that generates a uniform magnetic field over a small area. It is widely used. It is normally used for scientific experiments, magnetic calibration, and to cancel the background magnetic field in experiments. As shown in Figure 7, the ideal Helmholtz coil consists of a pair of circular coils with the same structure and size [7]. The planes of the coils are parallel to each other and the centers of the coils are on the same axis. The distance D between the center points of the coils is the same as the radius R of the coil itself. When the current goes through two coils in the same direction, it generates a uniform magnetic field in the volume within the coils. The axial magnetic field at the center is the sum of the axial magnetic field from two coils, and

$$\mathrm{B_z(z=0)} = \mathrm{N} \cdot \frac{8\mu_0 \mathrm{I}}{\sqrt{125}\mathrm{R}} \tag{1}$$

where N is the number of turns in the coil, R is the radius of the coil, and I is the current that goes through each coil. We will use a Helmholtz coil to generate the magnetic field in our proposed EUV light source. The design of the Helmholtz coil will be introduced in the chapter 3.

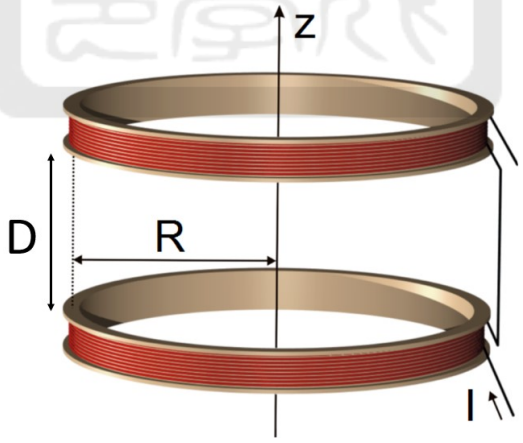

Figure 7: The Schematic of one-axis Helmholtz coil [7].

1.6 Our proposed EUV light source and the goal of the thesis

In Figure 8, we want to develop an EUV light source using a theta pinch, which belongs to the DPP. Compared with LPP, the way of DPP provides a higher overall conversion efficiency (CE) and is much cheaper. However, the lifetime of electrode is a big problem for DPP. For example, in the z-pinch EUV source experiment as shown in Figure 9 [8], the current not only flows through the plasma but also through the electrode surface. It caused the electrode getting eroded quickly. In order to diminish the problem, we decide to use the theta-pinch. It is because the coil that carries the current does not contact with the hot plasma directly in a theta-pinch.

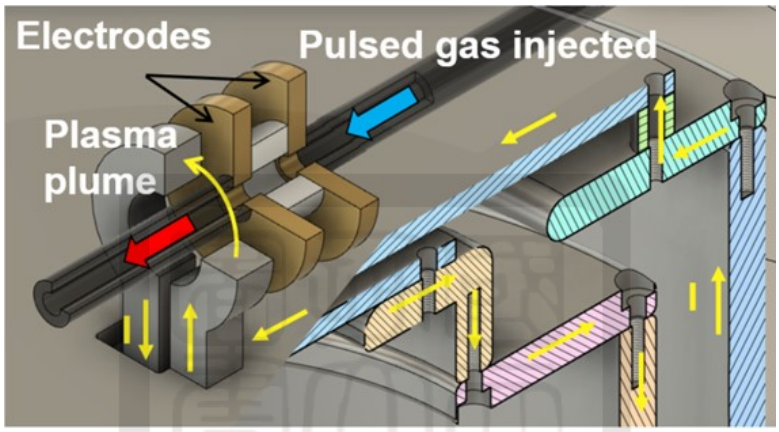

Figure 8: The schematic of our purposed EUV light source.

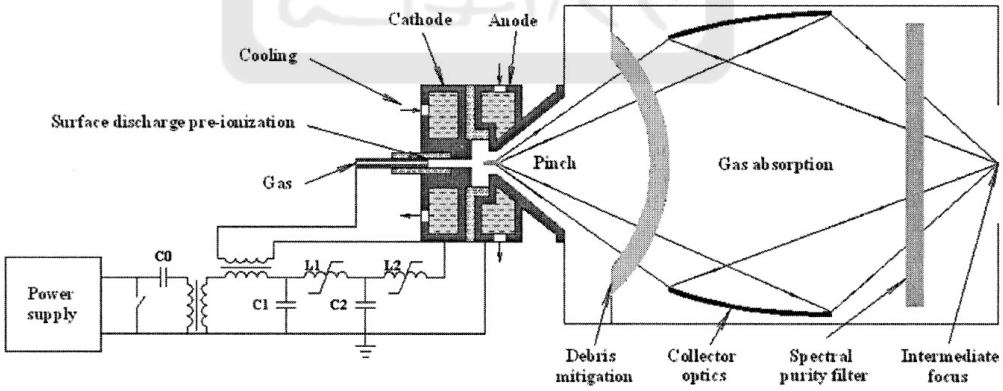

Figure 9: The schematic of z-pinch EUV source experiment [8].

The process of generating the EUV light is following. Initially, a gas puff is generated by a pulse valve. When the gas puff propagates to the gap between the pair of electrodes, an arc discharge is initiated by a self-breakdown. Then, a plasma plume is created from the gas puff. The plasma plume will arrive the center of the Helmholtz coil as shown in Figure 10. At this moment, the plasma is compressed by a theta-pinch driven by the pulsed-power system

adiabatically. Finally, the temperature of the plasma will reach ∼30 eV and radiating the EUV light.

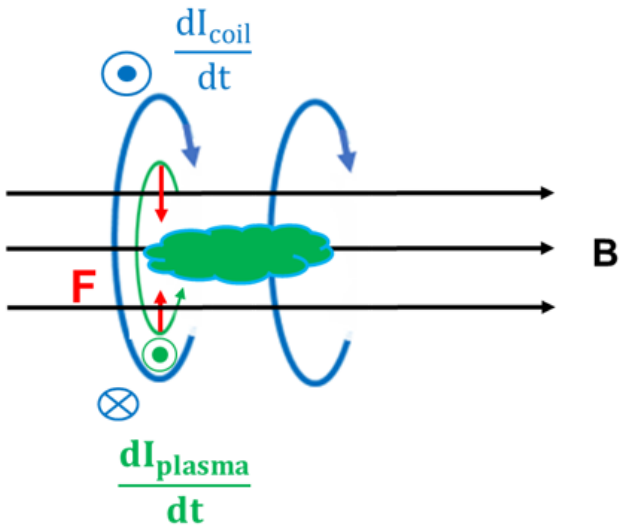

Figure 10: The schematic of the theta-pinch.

The goal of the thesis is to build a Helmholtz coil to provide the pulsed magnetic field for theta-pinch. Chapter 2 will describe the pulsed-power system and some components for experiments. In chapter 3, the design of the Helmholtz coil will be introduced. Then, we measured the magnetic field generated from the Helmholtz coil by using a B-dot probe. The design and the calibration of the B-dot probe will be given in chapter 4. In chapter 5, measurements of the magnetic field generated from Helmholtz coil discharge tests are given. Finally, future works and the summary are given in chapter 6 and chapter 7, respectively.

2 The pulsed-power system

The pulsed-power system is used to drive a Helmholtz coil to generate a pulsed magnetic field for compressing the plasma plume. In section 2.1, the structure of the pulsed-power system will be introduced. Since arc discharges often appeared in Helmholtz coil discharge tests, they caused the current signal of the Rogowski coil abnormal. After solving the arcing problem, we recalibrated the Rogowski coil for measuring the current of the system. The recalibration of the Rogowski coil is described in section 2.2. Further, over the past year, we integrated a Q-switch laser in our pulsed-power system to take images of plasma. We need to synchronize the triggering signal to the pulsed-power system with the flashlamp of the Q-switch laser using the timing fiducial signal. Therefore, I made a new optical trigger-pulse generator. It will be introduced in section 2.3.

2.1 The structure of the pulsed-power system

Our pulsed-power system consists of twenty 1-μF capacitors, two rail-gap switches, two parallel-plate transmission lines, and a cylindrical vacuum chamber orientated vertically. Figure 11 is the computer aided design (CAD) drawing of the system. Two capacitors are first connected in series forming a brick. Five bricks are connected in parallel forming a wing. The capacitor bank is divided in two groups which are the "north wing" and the "south wing." Finally, two wings are connected in parallel providing a capacitance of 5 μF in total [9].

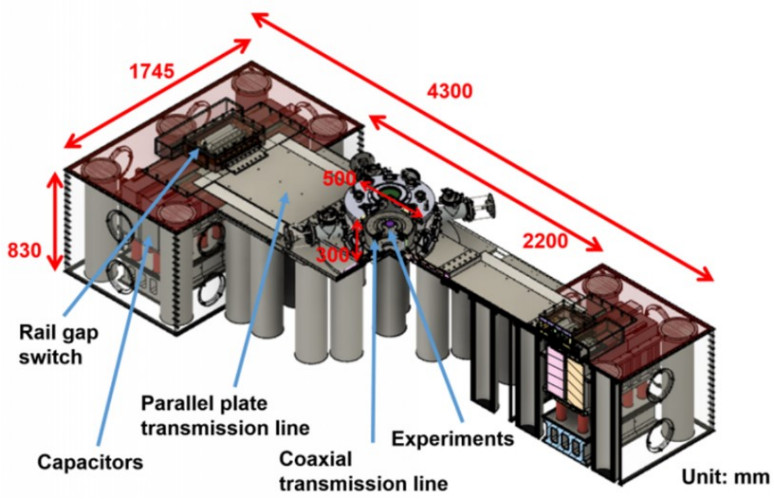

Figure 11: The CAD drawing of the pulsed-power system.

The discharge current is conducted through the parallel-plate transmission line and the coaxial-transmission line to the center of the cylindrical vacuum chamber for experiments as shown in Figure 12. The system is charged to 20 kV. When it is discharged, a peak current of 135 $\pm$1 kA with a rise time of 1592 $\pm$ 3 ns is generated [10]. The inductance and the resistance of the system obtained from the discharge tests are 204 $\pm$ 4 nH and 10.0 $\pm$ 0.2 mΩ, respectively. The current is used to drive the Helmholtz coil for generating a pulsed magnetic field.

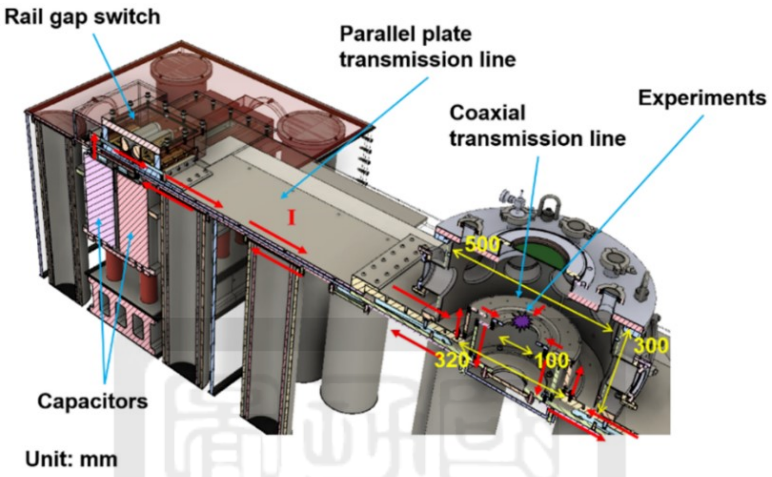

Figure 12: A half of pulsed-power system.

2.2 The recalibration of the Rogowski coil

In our experiments, we use the huge discharge current ∼130 kA provided by the pulsed-power system. However, we can't use the conventional current monitor to measure the current directly. Therefore, we use a Rogowski coil that is made by the former student, Jia-Kai Liu, as shown in Figure 13 [11]. It is an electrical device for measuring alternating currents (AC) or high-speed current pulses.

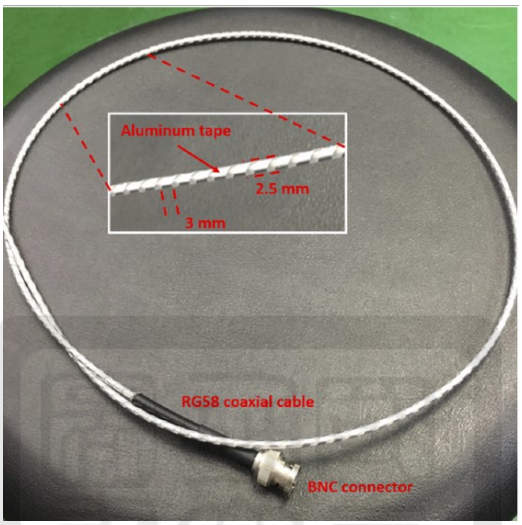

Figure 13: The photo of the Rogowski coil [11].

The Rogowski coil was made by a RG58 coaxial that was wrapped around with an aluminum tape as the helical coil. As shown in Figure 14, based on Faraday's law of electromagnetic induction, when the measured current I_{in} passes through the Rogowski coil, an induced voltage V_{out} at the output of the Rogowski coil is generated. The induced voltage in the coil is proportional to the rate of change of the measured current:

$$V_{out} = M_{\text{Rogowski coil}} \times \frac{dI_{in}}{dt}. \tag{2}$$

where $M_{\text{Rogowski coil}} = -\frac{r^2 N \mu_0}{2L}$ is the mutual inductance of the Rogowski coil. L is the radius of the Rogowski coil. r is the radius of each loop of the helical coil of the Rogowski coil. N is the number of turns of the Rogowski coil.

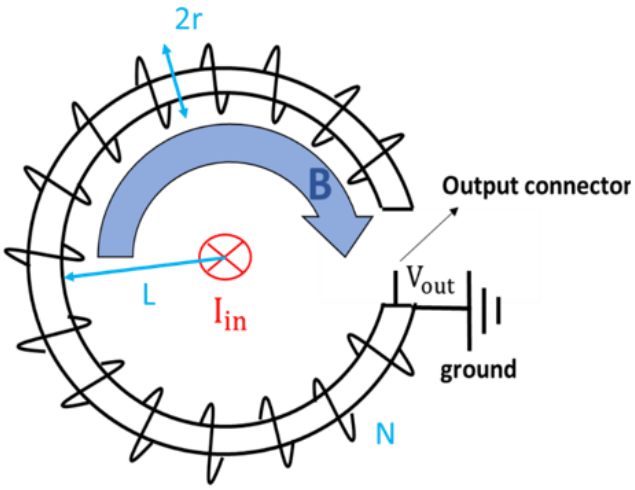

Figure 14: The schematic of Rogowski coil.

We place the Rogowski coil in the chamber of the pulsed-power system. It is located between two cylindrical coaxial transmission line (CTL). In order to transmit the V_{out}, the output connector of the Rogowski coil is fed out through the top plate of the CTL as shown in Figure 15. Then, we integrate the V_{out} with an RC integrator. The resistance and the capacitance of the RC integrator are 5 kΩ and 48 nF, respectively. The original conversion ratio between the voltage output of the Rogowski coil with the integrator V_R and the discharge current is 188.0±0.3 kA/V [12]. Therefore, we can get the discharge current I of the pulsed-power system directly by using equation (3).

$$I(\mathrm{kA}) = (188 \pm 0.3) \times V_R(\mathrm{V}). \tag{3}$$

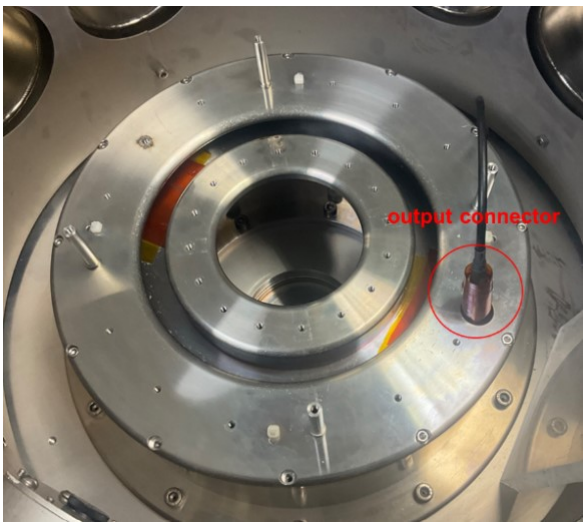

Figure 15: The output connector is fed out through the top plate of the CTL.

In Helmholtz coil discharge test, we found that the discharge current signal was often abnormal as shown in Figure 16. Normally, the discharge current behaves as an underdamped oscillation, e.g., the blue curve in Figure 16. On the contrary, the abnormal discharge current does not behave like an underdamped oscillation, e.g., the orange curve in Figure 16.

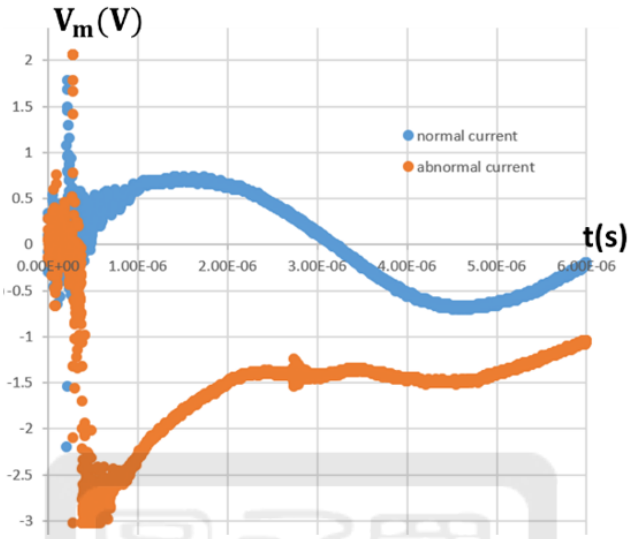

Figure 16: The normal discharge current and the abnormal discharge current.

We suspected that somewhere was arcing between the Rogowski coil output connector and the top plate of the CTL since the gap between them was very small. Therefore, we wanted to prevent the arcing between them. We used heat shrink tubes and Kapton tapes to cover the output connector. We also used Kapton tapes to cover the edge of the hole on the top plate of the CTL for feeding through the output connector. Then, the Rogowski coil was put back to the pulsed-power system. We decided to recalibrate the Rogowski coil with the Pearson current monitor (model 301x). In Figure 17, we used four wires as the load in the system for recalibration. The wires were connected between the outer cylinder of the CTL and the inner cylinder of the CTL. The wires passed through the Pearson current monitor and we could measure the current which flow through the wires. However, the maximum peak current allowed for the Pearson current monitor was 50 kA. Therefore, we only used the south wing of the pulsed-power system which provided a current of only a half of that provided by the whole system, i.e. $\sim$50 kA. Then, in order to measure the large current, we connected the output of the Pearson current monitor with a 50 Ω resistor in parallel and two 20 dB attenuator in series. The 50 Ω resistor connected in parallel supposes to reduce the output voltage of the Pearson monitor by half. However, we found that the measured current was larger than the actual value

due to the impedance mismatch between the Pearson monitor connected with a 50 Ω resistor in parallel and the 50 Ω coaxial cable. After several tests, we found that the reading from the Pearson monitor needed to be divided by 1.327±0.002.

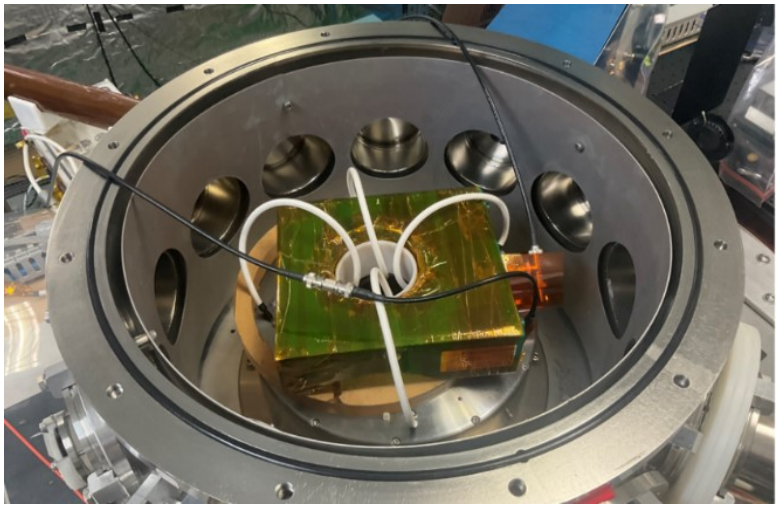

Figure 17: The calibration of the Rogowski coil with the current monitor.

Figure 18 is one of the experimental results for calibrating the Rogowski coil. The solid blue line is the voltage V_R of the Rogowski coil with the integrator. The red dash line is the current I_m measured by the Pearson current monitor. Next, we plotted the relationship between V_R in x-axis and I_m in y-axis in Figure 19. The slope is the calibration ratio. The new calibration ratio is 137.4±0.4 kA/V. The timing offset is 136±1 ns. The result is used for the rest of experiments. Figure 20 is the discharge current of the pulsed-power system. The load is four wires. The peak of the discharge current is ∼100 kA. The result matches the theoretical current $I = \frac{V}{\sqrt{L/C}} = \frac{20\,\mathrm{kV}}{\sqrt{205\,\mathrm{nH}/5\,\mu\mathrm{H}}} = 98.7\,\mathrm{kA}$ of the pulsed-power system.

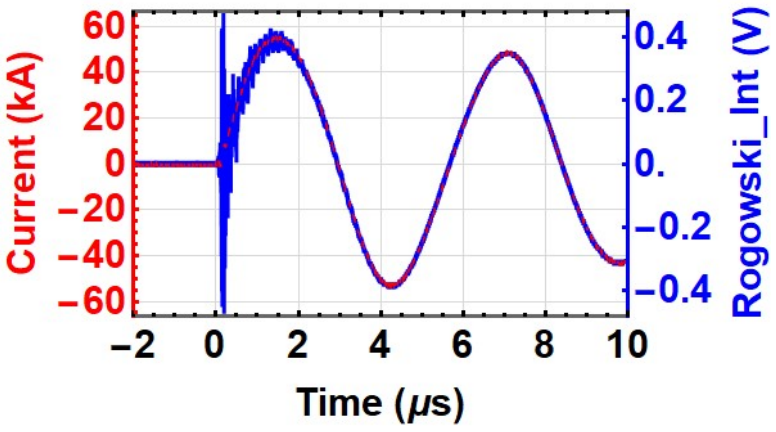

Figure 18: The calibration of the Rogowski coil.

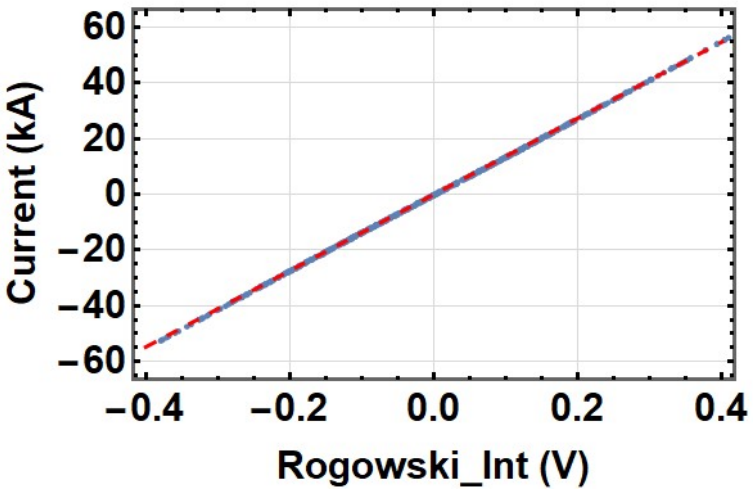

Figure 19: The relation between the I_m and V_R.

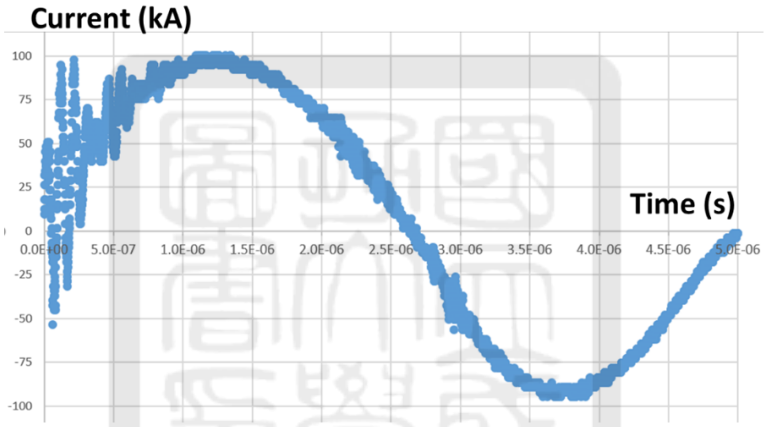

Figure 20: The discharge current of the pulsed-power system.

2.3 The new optical trigger-pulse generator

As shown in Figure 21, a Q-switch laser (Q-smart 850-2w SLM) was integrated in the pulsed-power system this year. It is used to take time-resolved images of plasma since it generates a burst of laser light with a pulse width of ∼5 ns. The gain media of the laser is pumped by a flashlamp. The flashlamp needs to flash with a frequency of 10 Hz to provide a stable laser output. Therefore, a function generator is used to generate a 10-Hz Transistor-transistor logic (TTL) signal with a pulse width of 35 μs as the timing fiducial signal. The flashlamp of the laser is synchronized with the timing fiducial signal for providing the stable laser output.

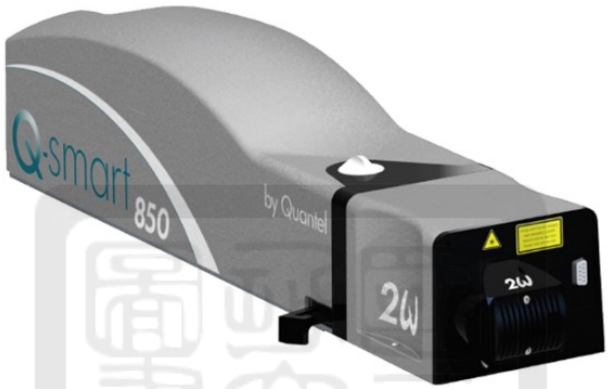

Figure 21: The Q-switch laser (Q-smart 850-2w SLM) [13].

On the other hand, the Q-switch needs to be activated to generate the burst of the laser light. The time difference between triggering the Q-switch and triggering the flashlamp controls the energy output of the laser. After testing, we have the Q-switch triggering signal 390 μs after the flashlamp triggering signal to produce the proper energy output. In addition, the Q-switch signal needs to be synchronized with the pulsed-power system so that images are taken at the right time.

In order to synchronize all signals, we design a new optical trigger-pulse generator to trigger the pulsed-power system first. Then, we use the pickup coil to pick up the time that the pulsed-power system is activated. Finally, we use the picked up signal to trigger the Q-switch laser with a proper delay provided by a delay generator DG645 made by Stanford research system, Inc. The flow chart of triggering the system is shown in Figure 22.

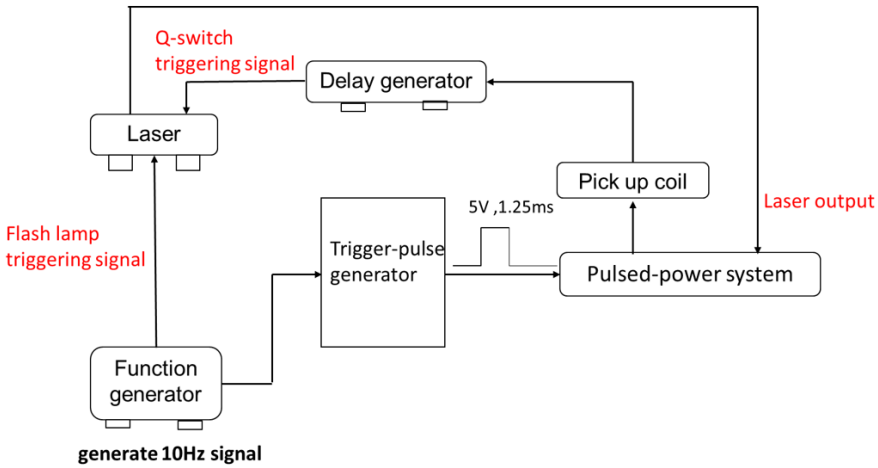

Figure 22: The flow chart of triggering the system.

First, we need to know the time delay of triggering the pulsed-power system. The time sequence of triggering the pulsed-power system is shown in Figure 23 [14]. At the beginning, a square optical trigger-pulse signal with a width of 1250 μs is generated by the optical trigger-pulse generator. A slow high-voltage pulse is generated 55 μs after the square optical trigger-pulse signal with a jitter of $\pm$400 ns. Then, the fast high-voltage pulse is generated a couple of nanoseconds after the slow high-voltage pulse is generated. Finally, the pulsed-power system is triggered by the fast high-voltage pulse after a couple of nanoseconds. In other words, it takes $\sim$1305.5 μs to trigger the pulsed-power system and the peak current is generated 1.6 μs after the pulsed-power system is triggered. Therefore, the Q-switch needs to be triggered $\sim$1.6 μs after the pulsed-power system is activated. The 1.6-μs delay can be controlled by the delay generator so that we can take images at different time. Notice that the flash lamp should flash $\sim$390 μs before the Q-switch is triggered.

In order to synchronize the pulsed-power system to the 10-Hz timing fiducial signal, the new optical trigger-pulse generator listens to the 10 Hz signal from the function generator. When the fire button of the new optical trigger-pulse generator is pressed, it will wait for the first timing fiducial signal after the fire button is pressed. Then, the 1250-μs square optical trigger-pulse signal is sent out 99084 μs after that timing fiducial signal, i.e., 916 μs before the following timing fiducial signal. Thus, the Q-switch signal of the Q-switch laser is synchronized to the current output. On the other hand, the time difference between the Q-switch signal and the flashlamp is 1305.5+Δt-916$\approx$390 (μs). ln experiments, the delay generator DG645 is used to provide the required delay Δt to trigger the Q-switch laser so that we can take the image at

a specific time.

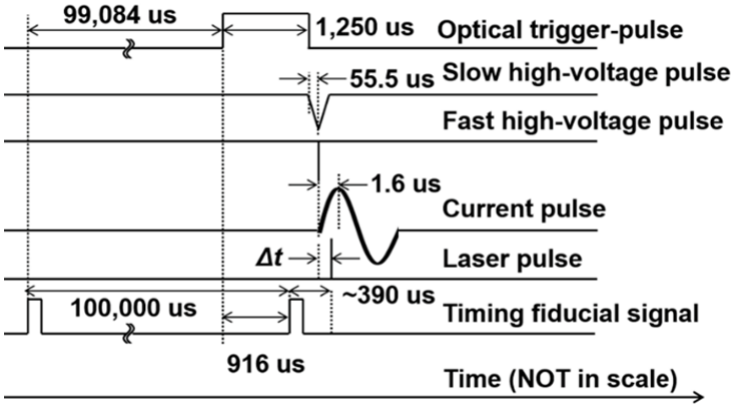

Figure 23: The time sequence of triggering the system [14].

2.3.1 The operation of the new optical trigger-pulse generator

The new optical trigger-pulse generator has two mode: "normal" mode and "Laser" mode. The "normal" mode is the use of the new optical trigger-pulse generator without using the laser. The system is in this state when the toggle switch SW-Laser is at "OFF" state. Contrarily, when the toggle switch (SW-Laser) is switched at "ON" state, the system is in the "Laser" mode. The "Laser" mode is chosen when we need to take time-resolved images of plasma with the laser. Figure 24 shows the flow chart. When we press the fire button of the new optical trigger-pulse generator when it is at "Ready to fire" state, it will send out one 1250-μs optical trigger-pulse 99084 μs after the first timing fiducial signal of the 10-Hz of the function generator if it is in the "Laser" mode. On the contrary, it will directly send out the 1250-μs optical trigger-pulse in the "normal" mode. The code of the new optical trigger-pulse generator is given in Appendix 1.

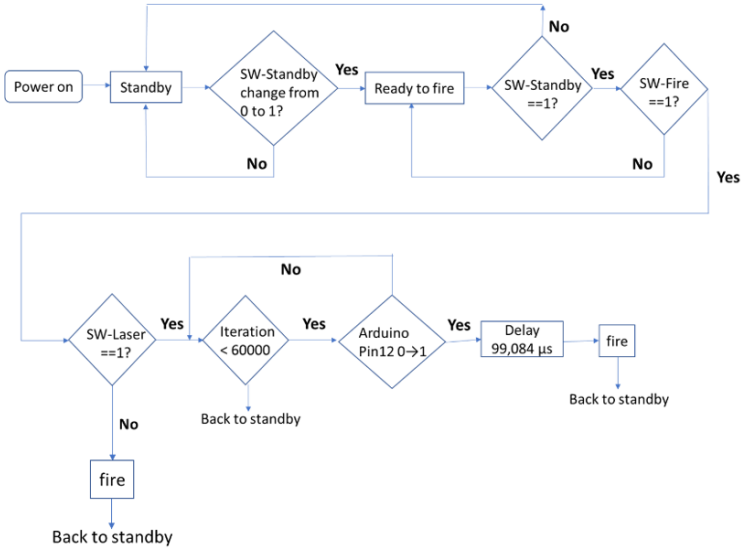

Figure 24: The flow chart of the new optical trigger-pulse generator.

2.3.2 The design of the new optical trigger-pulse generator

The original optical trigger-pulse generator, which is made by the former student, Yen-cheng Lin, is the initiator for our pulsed-power system. In order to synchronize the trigger pulse to the 10-Hz timing fiducial, I added some components. The added components are:

1. One switch for Laser (SW-Laser).
2. One LED for Laser (LaserLED).
3. The pin12 of Arduino-nano board is used for listening the 10-Hz timing fiducial signal from the function generator.

Figure 25 is the new optical trigger-pulse generator. Shown in Figure 26 is the circuit of the new optical trigger-pulse generator. An Arduino-nano board is used as the main component of the new trigger-pulse generator. The Arduino-nano board is suitable to generate the 1250-μs pulse. The optical signal is sent out via the fiber transmitter (HFBR-1528Z) and fiber. The board is preprogrammed to be controlled by switch buttons, to control LED indicators providing the information of different modes of the generator, and to provide the pulse. Three switches, two toggle switches as the "SW-Standby" and "SW-Laser", and one push button switch as "SW-Fire."

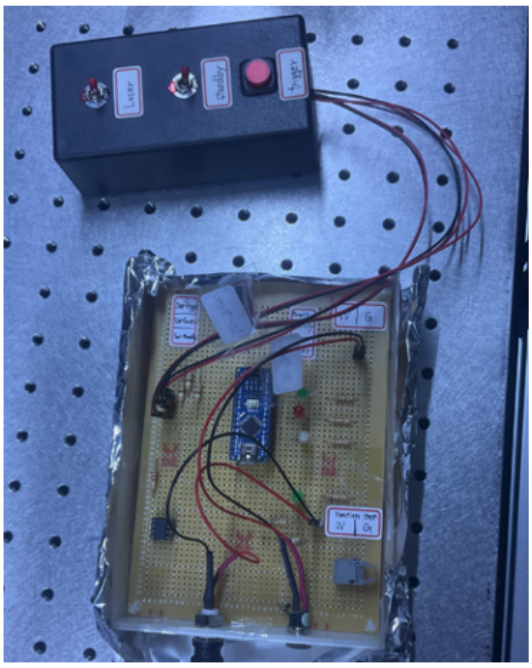

Figure 25: The photo of the new optical trigger-pulse generator.

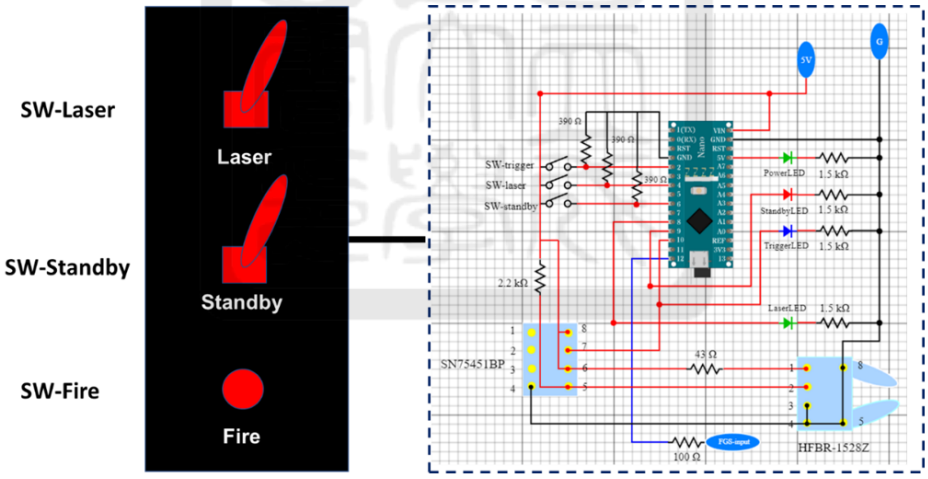

Figure 26: The circuit of the new optical trigger-pulse generator.

2.3.3 The test of the new optical trigger-pulse generator

Before we use the new optical trigger-pulse generator for triggering the pulsed power system for experiments, we have to make sure whether it works as expected or not. We need to check if the time difference between the timing fiducial signal from the function generator and the square pulse signal with a width of 1250 μs from the new optical trigger-pulse generator is as expected.

In Figure 27, a function generator was used to output a 10-Hz square pulse with a pulse width of 20 ms as the timing fiducial. The signal was sent to channel 1 (CH1) of the oscilloscope and the new optical trigger-pulse generator using a BNC T-connector. Then, we did the operation of "Laser" mode of the new optical trigger-pulse generator. Finally, the square pulse signal was sent to channel 3 (CH3) via a transmitter (O/E) because the square pulse signal was an optical signal and it needed to be converted back to the electrical signal.

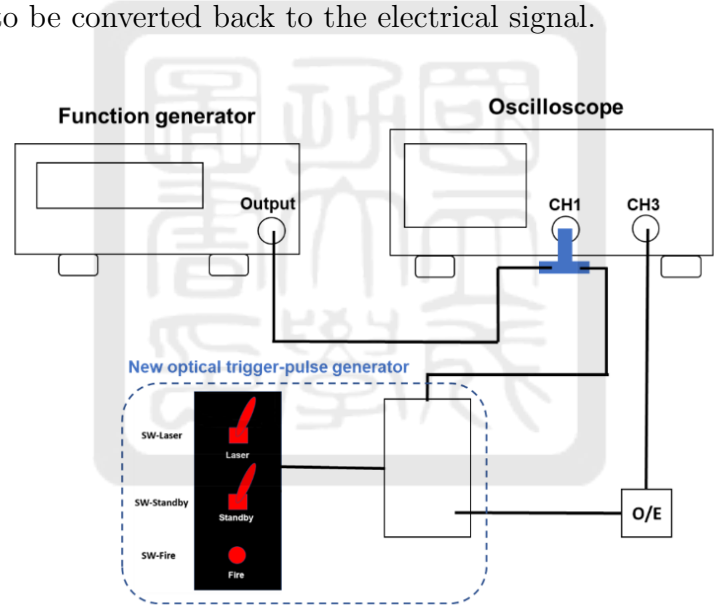

Figure 27: The experimental setup of the new optical trigger-pulse generator for testing.

In the test, when the "Fire button" of the new optical trigger pulse generator was pressed, it sent out a 1250-μs trigger-pulse signal 99084 μs after the first timing fiducial signal of after the button was pressed as shown in Figure 28. In other words, the 1250-μs trigger-pulse signal was sent 916 μs (Δt) before the following timing fiducial signal theoretically. Figure 29 is one of the data recorded by the oscilloscope. However, the time difference Δt had a jitter in the test. We got the time difference Δt from 7 shots. It was 822$\pm$7 μs. The data of 7 shots is listed in Table 1. Although it was different from 916 μs, we decided to use it to trigger the laser and

adjust the delay accordingly. Finally, we replaced the delay time 99084 μs by 99000 μs.

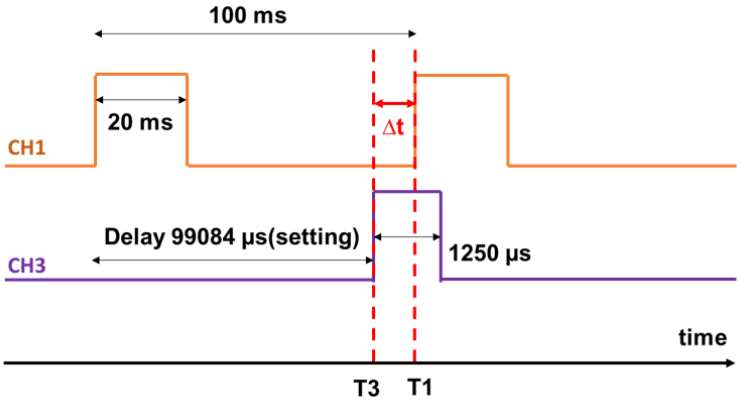

Figure 28: The time sequence of the 10-Hz signal (CH1) and 1250-μs trigger-pulse signal (CH3).

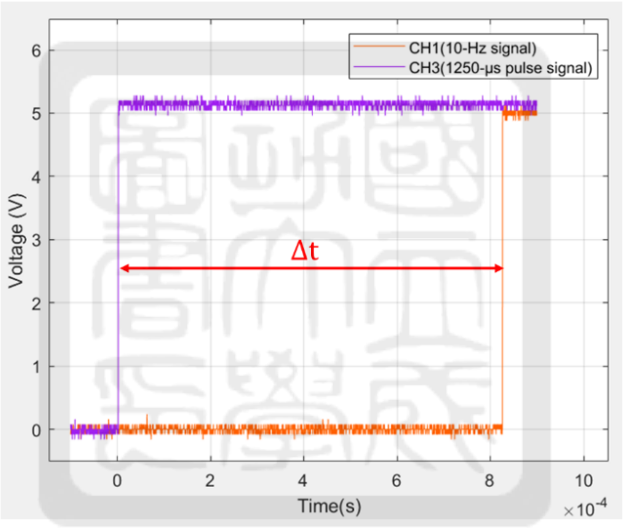

Figure 29: The result of one of 7 shots.

Table 1: The data of the test.

Data	T1(μs)	T3(μs)	Δt =T1-T3(μs)
1	826	2.8	823
2	814	2.8	811
3	825	2.8	822
4	818	2.8	815
5	830	2.8	827
6	836	2.8	833
7	827	2.8	824

2.3.4 The new optical trigger-pulse generator in experiments

The Q-switch laser is used to take the time-resolved images of the plasma jet of the bi-conical wire array at present [15]. In experiments, the laser would send out flashlamp triggering signals when it received the 10-Hz timing fiducial signal and the Q-switch triggering signal when the laser is fired. Figure 30 is one of the data recorded by the oscilloscope. The time difference between the two signals was ∼300 μs. Notice that the flashlamp of the Q-switch laser has an internal delay of 100 μs. In other words, the time difference between the flashlamp and the Q-switch is ∼300+100 ∼400 μs. It was ∼10 μs different from what we expected and was acceptable. In the future, the Q-switch laser will be used to take time-resolved images of the plasma plume in the theta pinch.

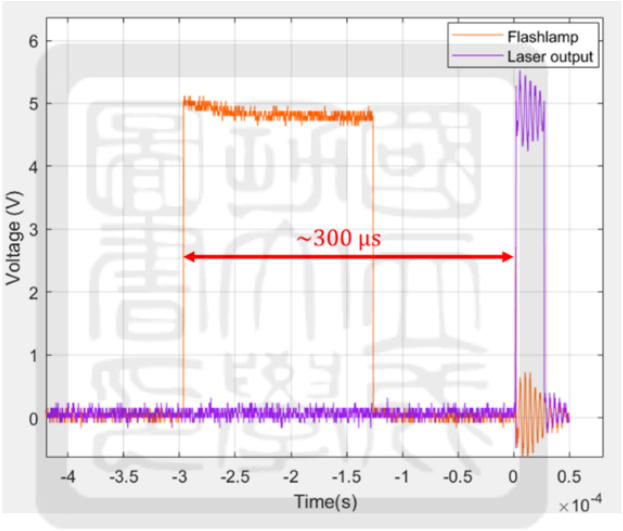

Figure 30: The time relation between the flash lamp signal and the laser output signal.

2.4 Summary

The pulsed-power system is the main experimental platform for driving the Helmholtz coil. The pulsed magnetic field that Helmholtz coil provides is used to compress the plasma plume in the future. In experiments, we measured the current of the pulsed-power system with a home-made Rogowski coil. However, the discharge current signal was often abnormal in the Helmholtz coil discharge test. The reason we suspected was the arcing between the Rogowski coil output connector and the top plate of the CTL. After putting more insulation using heat shrink tube and Kapton tape, the arcing problem was solved. We recalibrate the Rogowski coil with a Pearson monitor. The new calibration ratio is 137.4±0.4 kA/V with a time delay of 136±1 ns. Further, a Q-switch laser (Q-smart 850-2w SLM) was integrated this year. It is used to take time-resolved images of plasma. Therefore, a new optical trigger-pulse generator is used to synchronize all signals between the laser and pulsed-power system. In experiments, the time difference between the flashlamp and the Q-switch is ∼400 μs so that it provides a proper intensity. The laser is now synchronized with the pulsed-power system.

3 Helmholtz coil

We want to compress a plasma plume using a theta pinch. To compress the plasma plume, we plan to use a Helmholtz coil to provide the pulsed magnetic field as shown in Figure 31. Due to the geometry of the Helmholtz coil, we can easily inject the plasma plume into the center of the Helmholtz coil and diagnose the plasma from the side.

(a) (b)

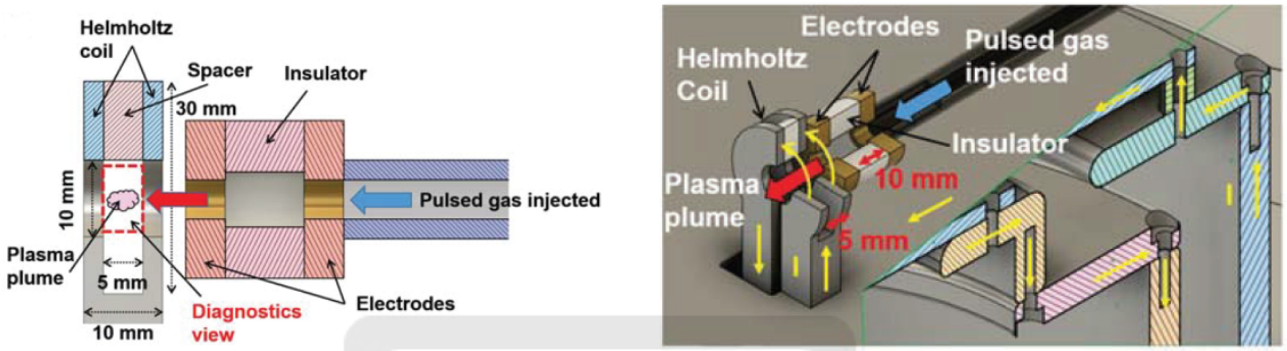

Figure 31: (a) The side view of the Helmholtz coil for the theta pinch. (b) The schematic of our proposed EUV light source.

3.1 The design of our Helmholtz coil

In our experiment, the Helmholtz coil is made of Stainless steel. The Helmholtz coil consists of two "coils," one "Helmholtz coil horizontal holder," and one "bottom coil connector" as shown in Figure 32.

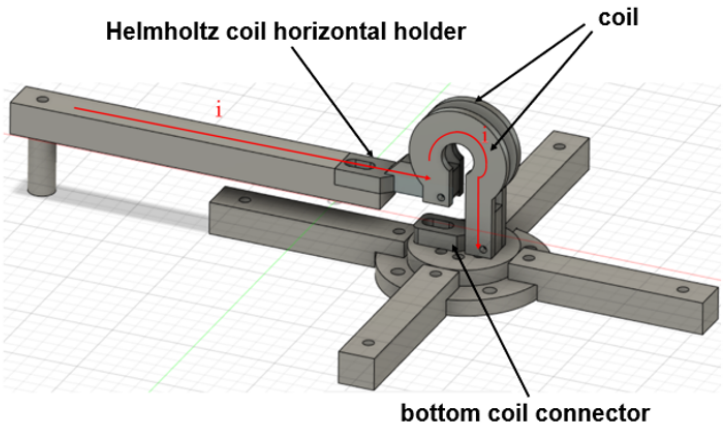

Figure 32: The CAD drawing of Helmholtz coil.

As shown in Figure 33, the inner radius of the Helmholtz coil is 5 mm and the outer radius is 15 mm. The separation between two coils is 5 mm. The Helmholtz coil which I designed is not a completed circle and the angle of the outer diameter is 270 degrees. The CAD design of Helmholtz coil is given in Appendix 2. Thus, it is not a typical Helmholtz coil so that the magnetic field may not be as uniform as the typical one.

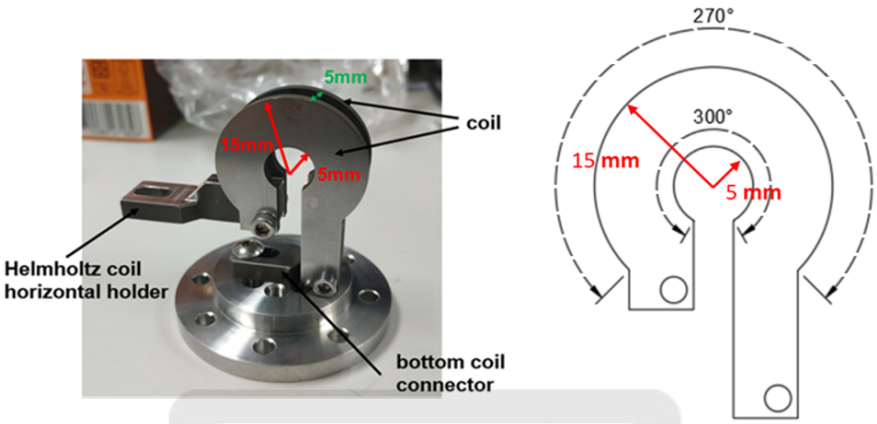

Figure 33: The structure of Helmholtz coil.

The Helmholtz coil is connected to our pulsed-power system. When the pulsed current flows through the Helmholtz coil, the coil may expand due to the Lorentz force. Shown in Figure 34, let T as the tension on the coil, R=5 mm as the inner radius of the coil, Δ=10 mm as the thickness of the coil, W=2.5 mm as the width of the coil, which is into the page and is not shown in the figure, and A =$\Delta\times$W as the area of the cross section of the coil. Therefore, to prevent the coil being exploded during the discharge, the magnetic pressure P_B needs to be balanced by the tension T of the coil, i.e., $R \times \theta \times W \times P_B = T \times \sin(\frac{\theta}{2}) \times 2 \approx T \times \theta$ for $\theta \to 0$,

$$\frac{T}{\Delta \cdot W} = \frac{R \cdot P_B}{\Delta} = \frac{R}{\Delta} \cdot \frac{B^2}{2\mu_0} = \frac{5}{10} \cdot \frac{B^2}{2\mu_0} \leq \text{Tensile strength of stainless steel.} \tag{4}$$

The tensile strength of stainless steel (AISI 302) is 520 MPa. Therefore, the Helmholtz coil can theoretically hold the magnetic pressure $P_B = \frac{B^2}{2\mu_0}$ of 1040 MPa, i.e., $B_{max} = 51T$.

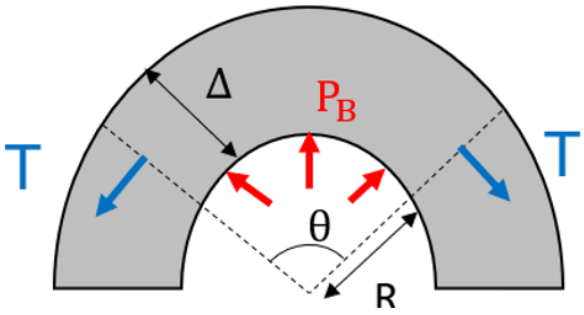

Figure 34: The relation between the tension on the coil T and the magnetic pressure P_B.

On the other hand, two coils are pushed toward each other by the Lorentz force as shown in Figure 35. A plastic spacer between two coils of the Helmholtz coil is used to prevent them crushing to each other as shown in Appendix 3. Then, we need to check that the Helmholtz coil can survive during the discharge. The Helmholtz coil discharge test will be introduced in Chapter 5.

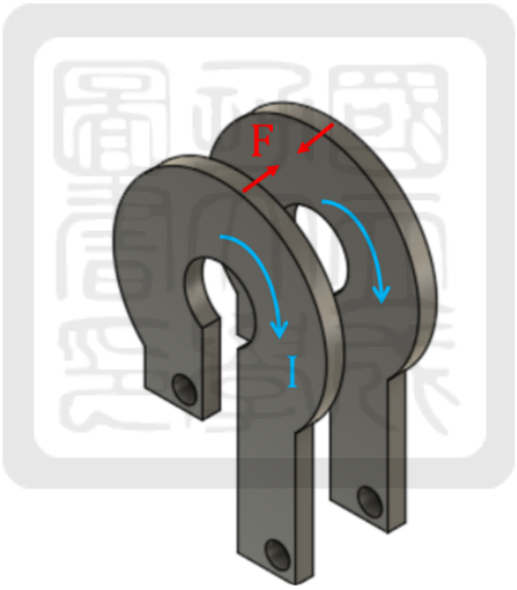

Figure 35: The Lorentz force F on two coils.

3.2 The theoretical magnetic field

To estimate the expected magnetic field, we have two ideal coils with a radius of 5 mm at -2.5 mm and +2.5 mm, respectively and let the 65-kA current flow through each coil. The 65-kA current is a half of the expected pulsed current provided by our pulsed-power system. The axial magnetic field distribution of this Helmholtz coil calculated using equation (5) is

$$B(z) = \frac{\mu_0 I R^2}{2[R^2 + (z + 2.5\,\mathrm{mm})^2]^{3/2}} + \frac{\mu_0 I R^2}{2[R^2 + (z - 2.5\,\mathrm{mm})^2]^{3/2}} \tag{5}$$

where R= 5 mm is the radius of the coil, and I=65 kA is the current that goes through each coil. The calculated result is shown in Figure 36.

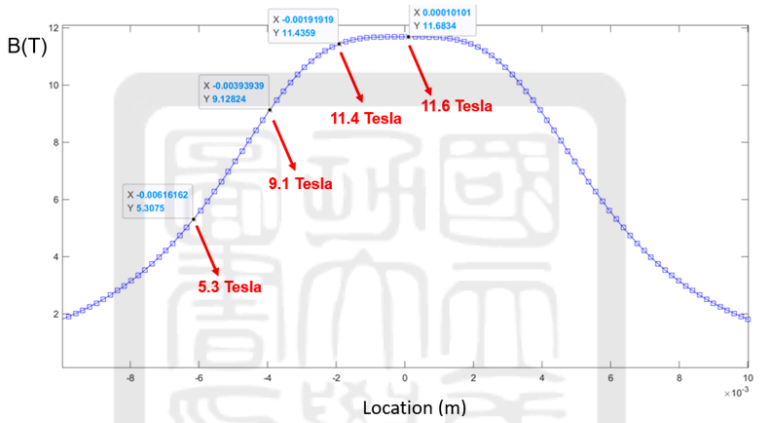

Figure 36: The axial magnetic field distribution of this Helmholtz coil.

The magnitude of the peak magnetic field at z=0 generated from the ideal Helmholtz coil is

$$B_0 = \frac{8\mu_0 I}{\sqrt{125}R} = \frac{8\mu_0 \cdot (65 \times 10^3)}{\sqrt{125} \cdot (5 \times 10^{-3})} = 11.6\,\mathrm{T}. \tag{6}$$

However, the Helmholtz coil which I designed is not an ideal Helmholtz coil. Since we don't know how the current is distributed in the coils, I calculated the magnetic field generated by two coils with different radius R and different separation d between them as shown in Figure 37. The formula of the magnetic field at z=0 generated from the two coil is

$$B_z(z = 0) = 2 \times \frac{\mu_0 I R^2}{2[R^2 + (\frac{d}{2})^2]^{3/2}} \tag{7}$$

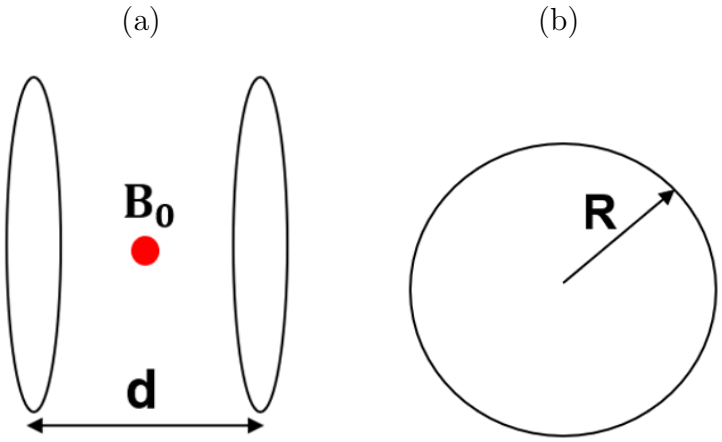

Figure 37: (a) The schematic of the two coils. (b) R is the radius of the coil.

Since the inner radius and the outer radius of my Helmholtz coil is 5 mm and 15mm, respectively. I have R=5, 10, 15 mm. On the other hand, the thickness of the coil is 2.5 mm and the separation between two coils is 5 mm. Therefore, I have d=5, 7.5, 10 mm. Finally, we calculate the magnetic field with different R and d and list them in Table 2. According to Table 2, the range of the ideal magnetic field generated from two coils is 4.6 $\sim$ 11.6 T.

Table 2: The ideal magnetic field generated from the two coils.

R(mm) / d(mm)	5	10	15
5	11.6 T	7.4 T	5.2 T
7.5	8.3 T	6.7 T	4.9 T
10	5.7 T	5.8 T	4.6 T

3.3 The simulated magnetic field

In addition to calculating the magnetic field of Helmholtz coil with ideal formula, I want to know the magnetic field of the coil with finite thickness. Therefore, I used a simulation software, COMSOL Multiphysics [16], to simulate the magnetic field generated from the Helmholtz coil.

3.3.1 Benchmark

First, in order to benchmark the simulation, I modeled a Helmholtz coil with small thickness, and compared the magnetic field distribution with that of an ideal Helmholtz coil with the same dimension. The magnetic field of the ideal Helmholtz coil is calculated using equation (5)

introduced in section 3.2.

Figure 38 demonstrates the structures of the Helmholtz coil with small thickness (0.05 mm). Finally, I compare the axial magnetic field of the simulation result with the theoretically calculated axial magnetic field as shown in Figure 39. We can see that the red curve (from simulation) is closed to the blue curve (from eq.5) indicating that the simulated magnetic field of the Helmholtz coil with small thickness (red curve) matches the theoretical magnetic field of the ideal Helmholtz coil (blue curve). Therefore, we know that the simulation result matches the theoretical calculation.

(a) (b)

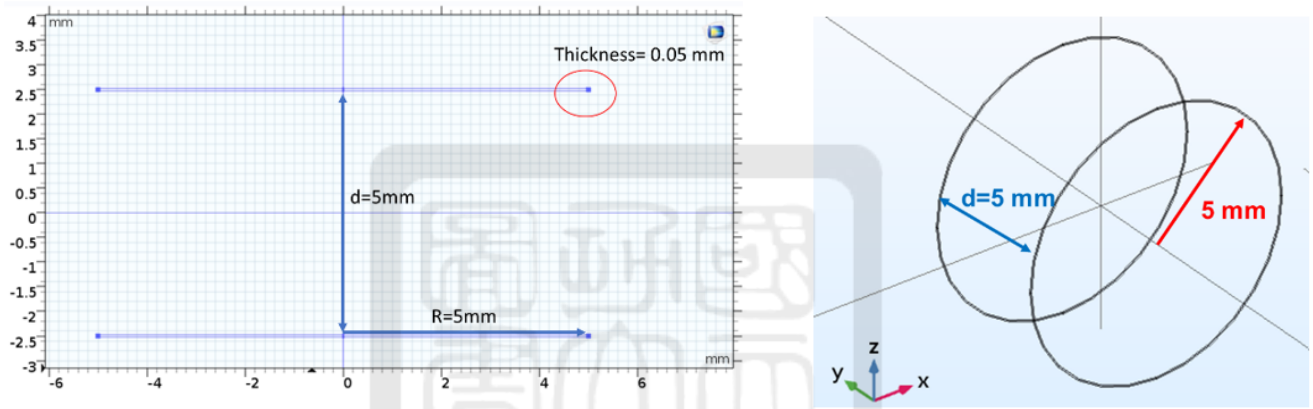

Figure 38: (a) The planar structure of the Helmholtz coil with small thickness. (b) The three-dimensional structure of the Helmholtz coil with small thickness.

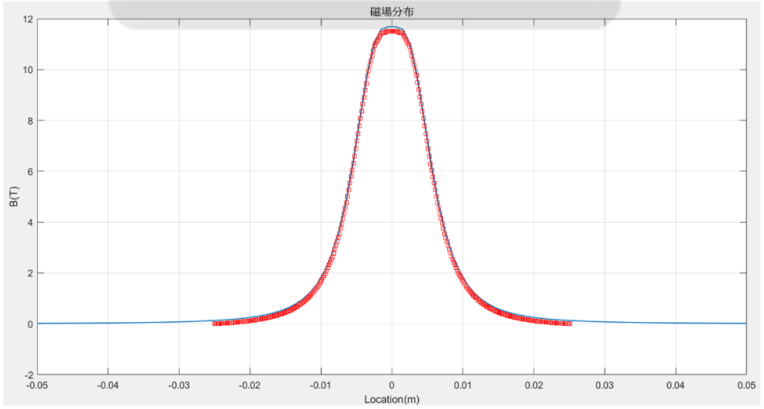

Figure 39: The comparison between the axial magnetic field of the simulation and the theoretical calculated axial magnetic field.

3.3.2 Simulated magnetic field of the actual Helmholtz coil

To be realistic, I simulate the Helmholtz coil whose dimension is the same as the Helmholtz coil which I designed introduced in section 3.1 as shown in Figure 40. I have the 65-kA current flows through each coil and let the current uniformly distributed in the cross section of the coil. The 3-D magnetic field distribution of the Helmholtz coil is shown in Figure 41. The gray structure is the Helmholtz coil. Since the direction of the current is clockwise, the direction of magnetic field (red arrow) is in the direction of +y. As shown in Figure 42, the peak magnetic field is 10.1 T. It should be the lower bound of the generated magnetic field.

(a) (b)

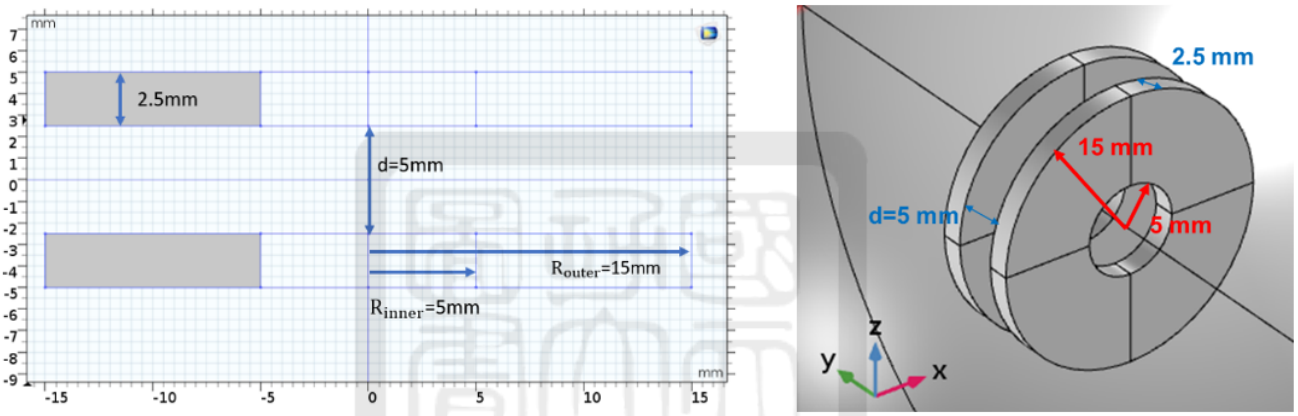

Figure 40: (a) The planar structure of the Helmholtz coil. (b)The three-dimensional structure of the Helmholtz coil.

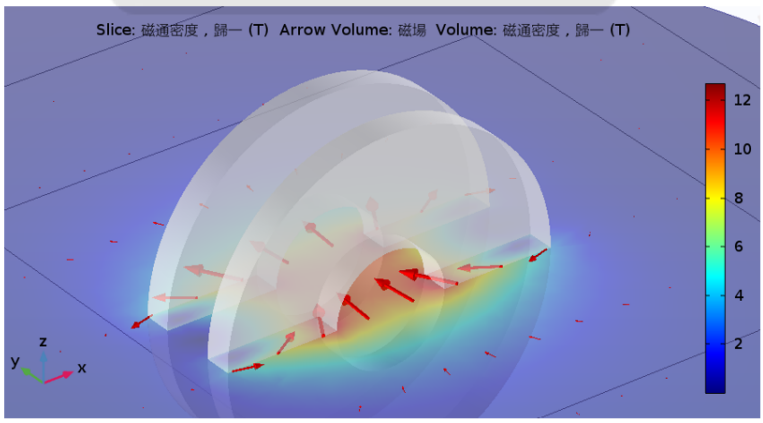

Figure 41: The magnetic field distribution of the Helmholtz coil.

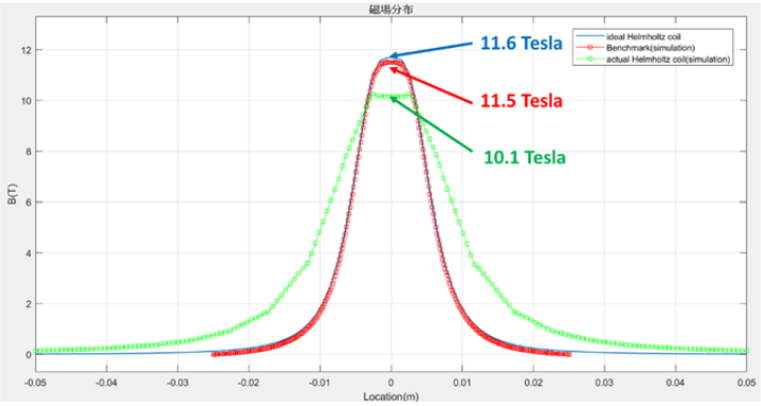

Figure 42: The comparison of magnetic field distribution.

3.4 Summary

To compress the plasma plume, the Helmholtz coil is used to provide the pulsed magnetic field for the theta pinch. The Helmholtz coil is made of Stainless steel. The Helmholtz coil consists of two "coils," one "Helmholtz coil horizontal holder," and one "bottom coil connector." The inner radius of the Helmholtz coil is 5 mm and the outer radius is 15 mm. The separation between two coils is 5 mm. The Helmholtz coil is connected to our pulsed-power system. When the pulsed current flows through the Helmholtz coil, two coils of Helmholtz coil may expand and be pushed toward each other due to the Lorentz force. Then, we need to check that the Helmholtz coil can survive during the discharge. When the 65-kA current flow through each coil, the range of the magnetic field at z=0 generated from Helmholtz coil is 4.6 $\sim$ 11.6 T. Additionally, we simulate the magnetic field generated from the Helmholtz coil with COMSOL. The magnetic field at z=0 is 10.1 T. It should be the lower bound of the generated magnetic field.

4 The B-dot probe

In our research, the magnetic field generated from the Helmholtz coil is important for the theta pinch. It needs to be measured. Thus, we decided to use the B-dot probe for measuring the magnetic field.

In many plasma experiments, the main parameters of the experiment include the magnitude of currents, magnetic and electric fields inside and outside the plasma. B-dot probes are electromagnetic sensors which are used to measure magnetic field in wide frequency ranges [17].

A B-dot probe is normally a coil made of an enameled copper wire. The operating principle of the B-dot probe is based on Faraday's law. When magnetic flux goes through the B-dot probe changes in time, an electromotive force V_{ind} is induced in the B-dot probe as shown in Figure 43. The magnitude of the induced voltage is proportional to the time derivative of the magnetic flux ϕ[18]:

$$V_{ind} = -\frac{d\phi}{dt} = -N \cdot \frac{d\int \vec{B} \cdot d\vec{A}}{dt} = -N \cdot A \frac{dB_{avg}}{dt} \tag{8}$$

where $\phi = N \cdot \int \vec{B} \cdot d\vec{A}$, and N is the number of turns of coils in the B-dot probe.

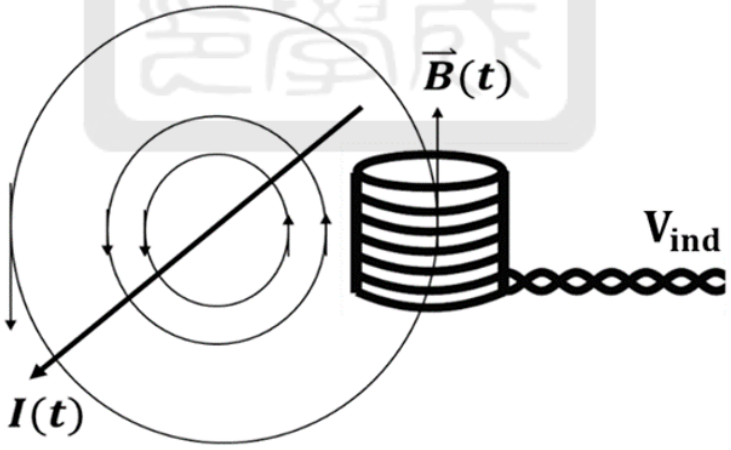

Figure 43: The schematic of the B-dot probe [18].

If the cross section of the B-dot probe is a constant in time, the averaged magnetic field sampled by the B-dot probe is given by $B_{avg} = \frac{\int \vec{B} \cdot d\vec{A}}{A}$,i.e.,

$$B_{avg} = -\frac{1}{NA} \int V_{ind} dt \equiv -C_{calib} \int V_{ind} dt \tag{9}$$

The calibration factor C_{calib} may not equal to $\frac{1}{NA}$ since the area A may have systematic error. Therefore, as long as we know the calibration factor C_{calib}, we can obtain the magnitude of the magnetic field at the location we measure by integrating the induced voltage of B-dot probe with time.

4.1 The design of the B-dot probe

In Figure 44, the B-dot probe is a single-turn coil which is made of enameled copper wires with a diameter of 0.5 mm. The B-dot probe has only one turn and the diameter of the B-dot probe is 5 mm. The terminals of B-dot probe are twisted forming a twisted pair. The twisted pair can reduce the attenuation and noise during transmission and improve the ability to suppress external electromagnetic interference [19]. The RG 58 coaxial cable is used to connect the terminals of the twisted pair of the B-dot probe to the oscilloscope.

Figure 44: The photo of the B-dot probe.

Therefore, we can observe the induced voltage on the B-dot probe directly from the oscilloscope. Finally, the magnetic field is obtained by integrating the induced voltage using a RC integrator in time as shown in Figure 45.

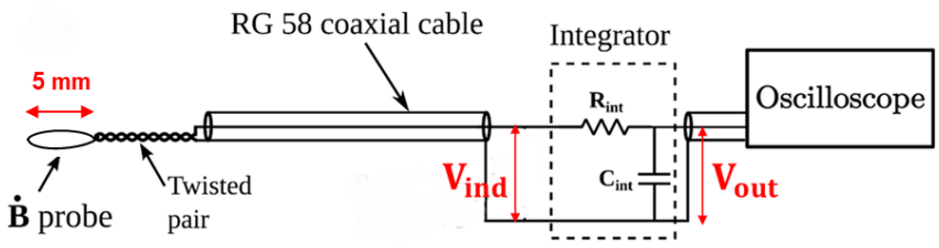

Figure 45: The B-dot probe with an integrator.

We used a section of enameled copper wire with a RG-58 coaxial cable to make the B-dot probe. The probe was fixed with a 3D-printed support. Figure 46 demonstrates how to make the B-dot probe. The procedure of making the B-dot probe is following:

1. Cut a section of enameled copper, fold it in half and put into the groove of the 3D-printed support.

2. Secure the B-dot probe in the 3D-printed support and remove the insulating layer on both ends of the enameled wire.

3. Twist the two ends of B-dot probe forming a twisted pair.

4. Remove the outer insulating layer near one end of the RG-58 coaxial cable. One end of the B-dot probe is connected to the center copper core of the RG-58 coaxial cable. The other end of the B-dot probe is connected to the braided conductive layer of the RG-58 coaxial cable.

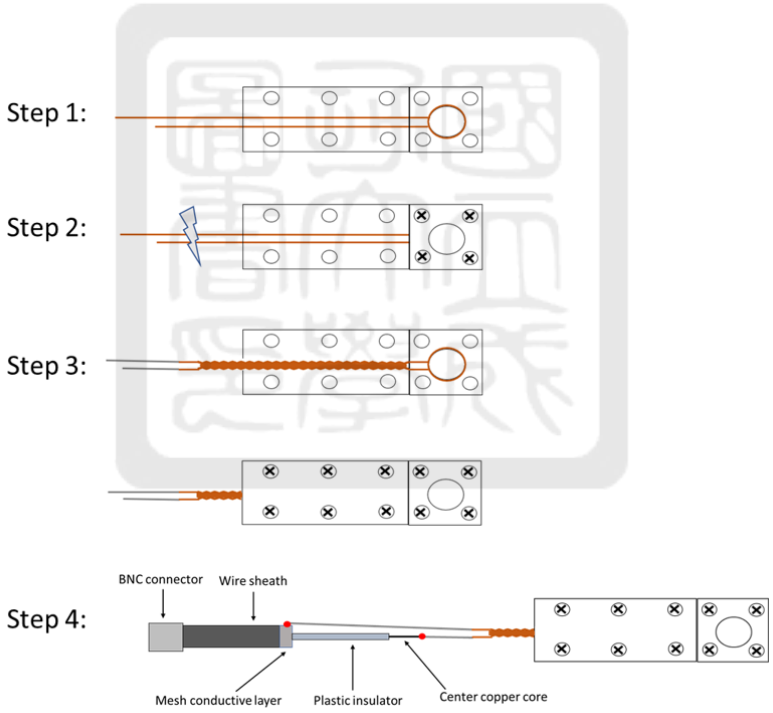

Figure 46: The production of the B-dot probe.

4.2 Calibration of the B-dot probe

Before using the B-dot probe to measure the magnetic field of the Helmholtz coil, the B-dot probe needs to be calibrated by a known magnetic field. A calibrated solenoid provides the known magnetic field for the calibration.

4.2.1 The magnetic field generated from a solenoid

We made a solenoid as shown in Figure 47 to generate a known magnetic field source. When the current passes through the solenoid, a uniform magnetic field is generated inside the solenoid. The solenoid is made of a PVC tube with a diameter of 34 mm and an electrical wire with a cross section of 1.25 mmˆ2. The length of the solenoid is 21 cm with 65 turns of coils in total. In other words, the number of turns per unit length (n) of the solenoid is 309.5 turns/m. The measured resistance and inductance are 0.1 Ω and 15.14 μH, respectively. They were measured by the RLC meter (LCR-6300, Good will Instrument Co. LTD). According to the formula of an ideal solenoid, the magnetic field inside this solenoid is

$$\mathrm{B(t)} = \mu_0 \cdot \mathrm{n\,I(t)} = \mu_0 \cdot 309.5\,\mathrm{I(t)} = 3.889 \times 10^{-4} \times \mathrm{I(t)}. \tag{10}$$

where μ_0 is the permeability of vacuum, I(t) is the current passes through the wire, and B(t) is the magnetic field generated inside the solenoid. However, equation (10) needs to be verified experimentally.

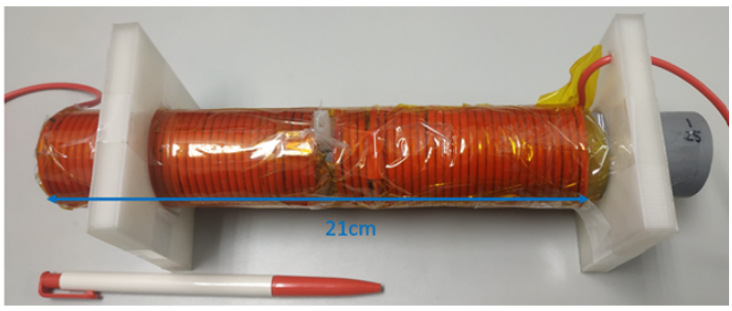

Figure 47: The picture of solenoid.

Additionally, in order to measure the magnetic field inside the solenoid, I drilled a hole on the solenoid and put the probe of the Gauss meter (FWBELL-5180 or WT10A by WEITE MAGNETIC) into the hole. The direction of the magnetic field lines of the measured magnetic

field is perpendicular to the Hall element at the front end of the probe of the Gauss meter as shown in Figure 48. To make sure that every time when we measure the magnetic field, the probe is inserted to the same location, I made a support using the 3D printer as shown in Figure 49. The CAD drawing of the support is provided in Appendix 4. The support is first inserted through the hole on the side of the solenoid into the solenoid. Then, the probe of the Gauss meter is inserted into the support. In Figure 50, the probe (red dash square) is fixed inside the solenoid and the sensor (blue circle) on the probe is at the center of the cross section of the solenoid.

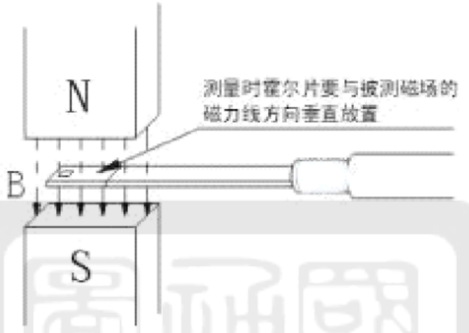

Figure 48: The way to measure the magnetic field with the Gauss meter [20].

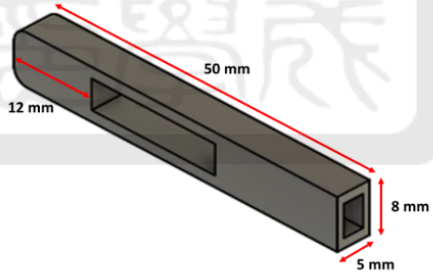

Figure 49: The CAD drawing of the support.

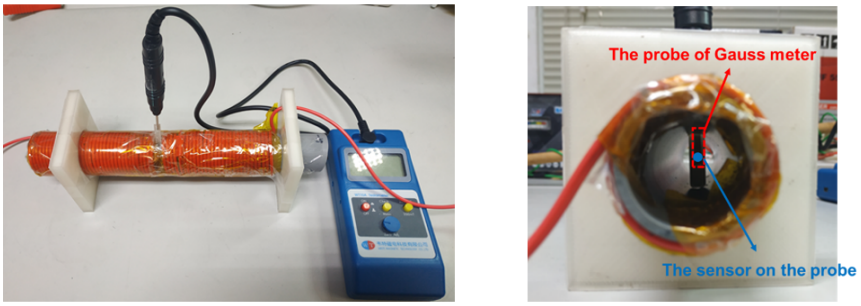

Figure 50: The probe of the Gauss meter is fixed in the center of the circular section of the solenoid.

A direct current (DC) was delivered to the solenoid for generating the magnetic field. The circuit that was used to produce DC current flowing through the solenoid is shown in Figure 51. In experiments, I adjusted the output voltage of the power supply and recorded the magnetic field displayed on the Gauss meter and the current displayed on the power supply simultaneously.

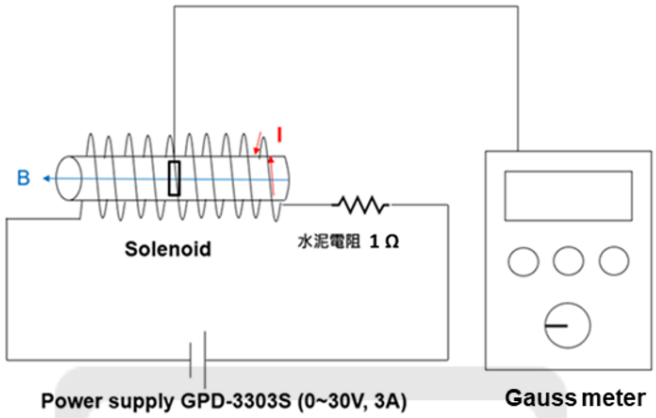

Figure 51: The circuit of the experimental setup.

The results of the magnetic field inside the solenoid is shown in Figure 52. The formula of the fitted curve is

$$\mathrm{B} = (3.00 \pm 0.05) \cdot \mathrm{I} + (0.96 \pm 0.05)\ [\mathrm{G}] \approx 3 \times 10^{-4} \times \mathrm{I}\ [\mathrm{T}]. \tag{11}$$

Because a hole was drilled in the solenoid, it may result in a reduction and nonuniformity of the magnetic field. Therefore, the difference between equation (10) and equation (11) could be the nonuniformity in magnetic field inside the solenoid.

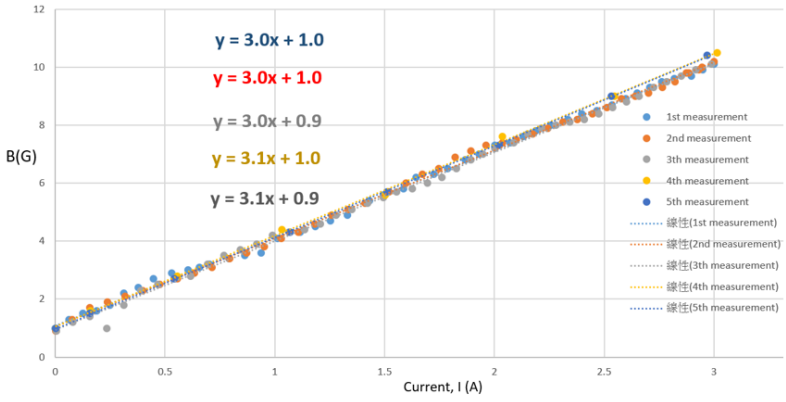

Figure 52: The results of the magnetic field generated inside the solenoid.

4.2.2 Calibration of the B-dot probe in a high-pulsed current

We want to know the calibration factor C_{calib} of the B-dot probe. When a high-pulsed current flows through the solenoid, the magnetic field inside the solenoid can be inferred. By comparing the induced voltage of the B-dot probe and the inferred magnetic field, we can obtain the C_{calib} in equation (9).

The setup of the experiment for calibrating the B-dot probe is shown in Figure 53. We use a high-voltage power supply to charge the 1-μF capacitor. When it is charged to $\sim$12 kV, the spark gap is activated via self-breakdown. A high-pulsed current of $\sim$2 kA is generated and flows through the solenoid. Then, the pulsed magnetic field B(t) is generated from the solenoid. I put the B-dot probe inside the solenoid and we measure the induced voltage. In addition, the current is measured by the Pearson current monitor (model 301x). We can infer the magnetic field by using equation (11).

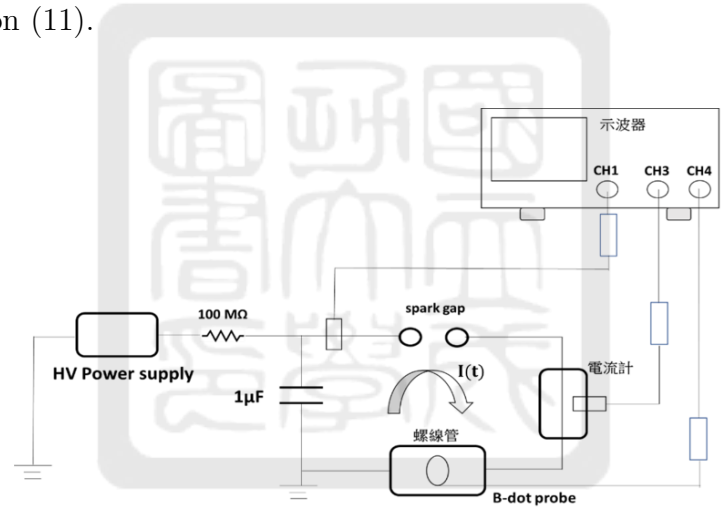

Figure 53: The calibration of the B-dot probe.

In each experiment, we measured the current from the output of the Pearson current monitor and the output of the B-dot probe on the oscilloscope at the same time. Figure 54 is one of the raw data of the discharge current and the induced voltage of the B-dot probe. The yellow data is the current measured by the Pearson current monitor while the green data is the induced voltage of the B-dot probe. The induced voltage is related to the derivative of the current. We used equation (12) and equation (13) to fit two curves:

$$I(t) = a \times e^{-[d(t-c)]} \sin[b(t-c)] + e = I_0 \times e^{-[d(t-c)]} \sin[b(t-c)] + e \qquad (12)$$

where I_0=2120 A, b=1.8×10^5 rad/s, c=-1.1×10^{-6}, and d=3271, and

$$V_{ind}(t) = -a \times b \times e^{-[d(t-c)]} \cos[b(t-c)] + a \times d \times e^{-[d(t-c)]} \sin[b(t-c)] \quad (13)$$

where a=1.552×10^{-5} , b=1.8×10^5 rad/s, c=-8.7×10^{-6}, and d=4040.

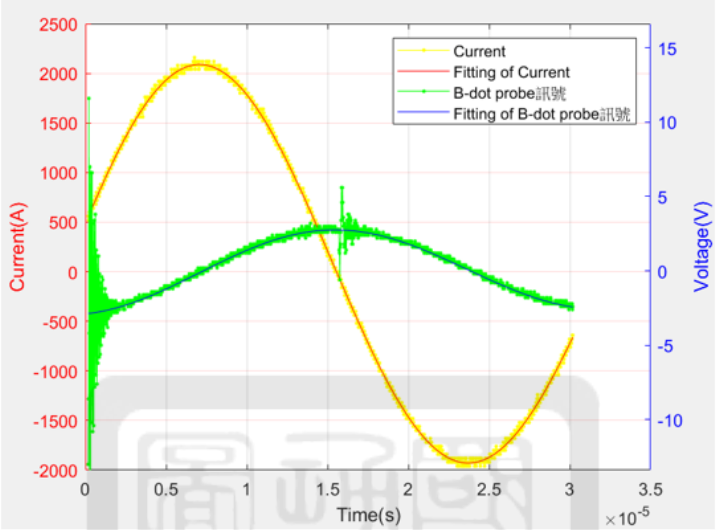

Figure 54: The raw data of the current and the induced voltage of the B-dot probe.

From equation (11), the inferred magnetic field is

$$B(t) = 3 \times 10^{-4} \times I(t) = 0.636 \times e^{-[d(t-c)]} \sin[b(t-c)] + e. \quad (14)$$

According to equation (9), $B_{avg} = -\frac{1}{NA} \int V_{ind} dt \equiv -C_{calib} \int V_{ind} dt$. In Figure 55, we plotted the relation between the $-\int V_{ind} dt$ in x axis and B(t) in y axis at different times. Notice that from equation (13), $-\int V_{ind} dt = a \times e^{-[d(t-c)]} \sin[b(t-c)]$. The slope of data in Figure 55 is the calibration ratio C_{calib} of the B-dot probe. Therefore, the calibration ratio of all data is 41500±300 (T/Vsec). The theoretical calibration factor C_{calib} is $\frac{1}{A} = \frac{1}{(2.5\times10^{-3})^2\times\pi}$=50929. The measured C_{calib} is 18.55% less than the theoretical value. The systematic error may come from the error of the coil radius. If it is the case, the error of the radius is 10%, i.e., 250 μm, larger than the designed radius. It is a reasonable error for a hand-made B-dot probe.

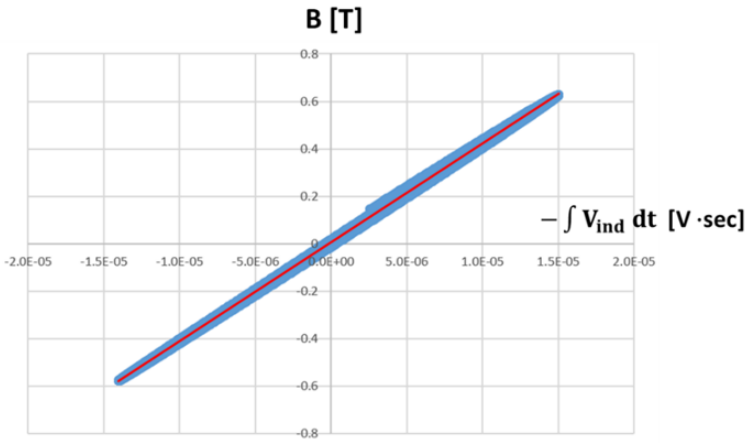

Figure 55: The relationship between the magnetic field and the integrated voltage.

4.2.3 The passive RC integrator

The passive RC integrator is used to integrate the induced voltage of the B-dot probe to get the measured magnetic field. In order to measure the magnetic field of the Helmholtz coil at two locations at the meantime, we made two RC integrator as shown in Figure 56. The information of the two RC integrator is listed in Table 3. Figure 57 shows the circuit diagram of the RC integrator. A resistor R is in series with a capacitor. The input voltage V_{in} is applied to the resistance and charges the capacitor. The capacitor charging current is written as

$$I_C(t) = C\frac{dV_c}{dt} = \frac{V_{in} - V_{out}}{R}. \tag{15}$$

Then, the output voltage comes from the voltage across the capacitor, we have

$$V_{out} = V_c = \frac{Q}{C} = \frac{1}{C}\int Idt. \tag{16}$$

If the time scale t of V_{in} is much shorter than the time constant $\tau = RC$, i.e. $t \ll \tau$,

$$V_{out} = \frac{1}{RC}\int_0^t V_{ind}dt. \tag{17}$$

Figure 56: The photo of the two RC integrator.

Table 3: The two RC integrator.

	R	C
RC integrator #1	5 kΩ	49 nF
RC integrator #2	5 kΩ	53 nF

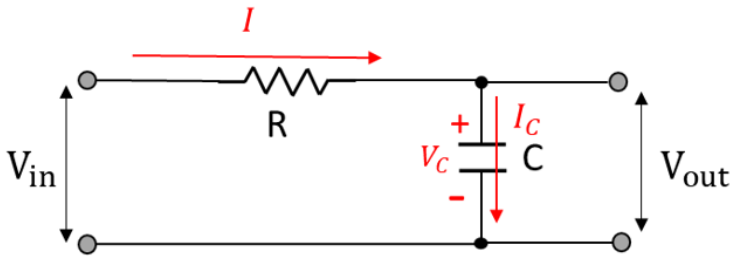

Figure 57: The circuit of the RC integrator.

In the calibration of the B-dot probe in a high-pulsed current, we used the RC integrator to integrate the induced voltage of the B-dot probe. The phase of the integrated voltage V_B matches the phase of the inferred magnetic field of the solenoid as shown in Figure 58. Then, we plotted relationship between the magnetic field B(t) in y-axis and the integrated voltage in x-axis as shown in Figure 59. The slope of data in Figure 59 is the calibration ratio of the B-dot probe with a RC integrator. The calibration ratio is 8.0±0.1 (Tesla/V). After we got the calibration ratio for both RC integrators, the measured magnetic field can be obtained from the B-dot probe with the RC integrator by using equation (18).

$$B_{measured} = (8.0 \pm 0.1) \times V_B(V). \tag{18}$$

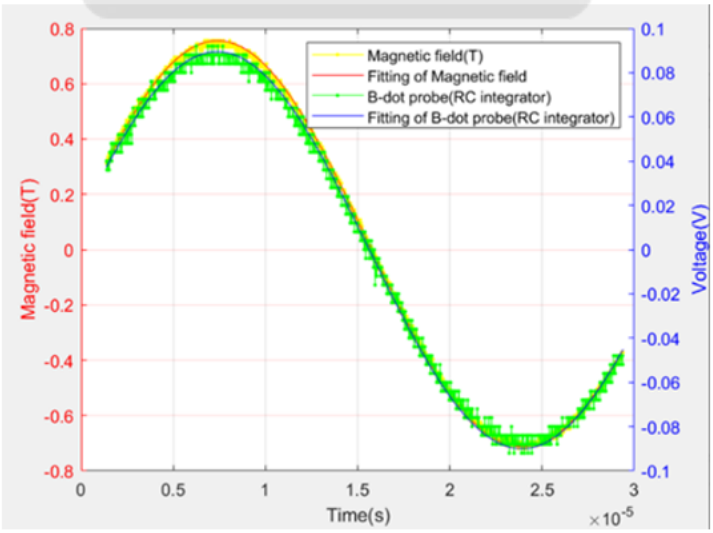

Figure 58: The inferred magnetic field and the voltage of the B-dot probe with a RC integrator.

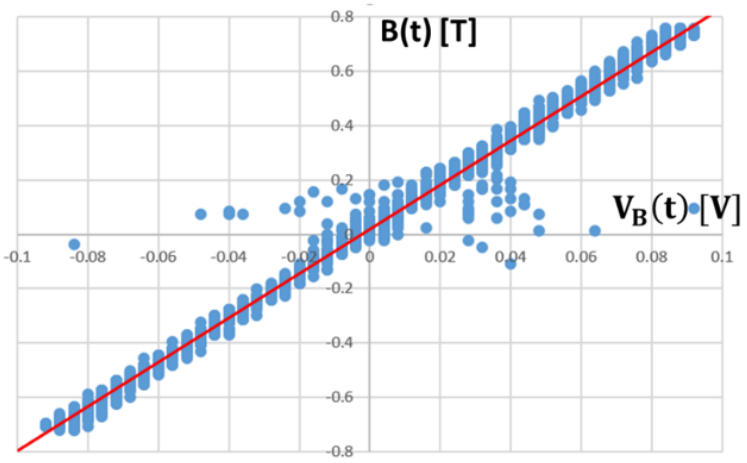

Figure 59: The relationship between the magnetic field and the voltage of the B-dot probe with a RC integrator.

4.3 Summary

In order to measure the magnetic field of the Helmholtz coil, we built the B-dot probe. The B-dot probe was a single-turn coil which was made of 0.5-mm enameled copper wires. The diameter of the B-dot probes was 5 mm. Before we measured the magnetic field of the Helmholtz coil, the B-dot probe was calibrated by a known magnetic field provided by a solenoid. The magnetic field generated from the solenoid was $B \approx 3 \times 10^{-4} \times I\,[T]$. Afterward, a pulsed current flowing through the solenoid for generating a pulsed magnetic field inside the solenoid was used to calibrate the B-dot probe. By comparing the induced voltage of the B-dot probe and the magnetic field of the solenoid, we obtained the conversion ratio C_{calib} in equation (9). The conversion ratio C_{calib} is 41500±300 (T/V·sec). Additionally, we made two RC integrators for integrating induced voltage of B-dot probes. We obtained the measured magnetic field from the B-dot probe with the RC integrators directly and got $B_{measured} = (8.0 \pm 0.1) \times V_B(V)$.

5 Helmholtz coil discharge tests

We measured the magnetic fields generated by the Helmholtz coil driven by the pulsed-power system. Before measuring the generated magnetic field, we tested the Helmholtz coil and see if it can survive after the discharge. We have tested the discharge under three conditions: discharge in atmosphere described in section 5.1, discharge under low vacuum given in section 5.2, and discharge under high vacuum provided in section 5.3. Finally, the field measurements are presented in section 5.4.

5.1 Discharge in atmosphere

We tested the Helmholtz coil in atmosphere first. We did not cover the vacuum chamber and observed the Helmholtz coil discharge directly from the top of the chamber. When the pulsed current flows through the Helmholtz coil, the coil may expand due to the Lorentz force. If the structure of the coil is not strong enough, the coil will be damaged. Therefore, we need to check whether the Helmholtz coil will survive after each discharge or not. In order to prevent the fragments of the broken coil from damaging the chamber, I placed a Polyvinyl Chloride (PVC) tube around the coil and put a transparent acrylic plate on the top as shown in Figure 60. In experiments, when the system was discharged, the large current flowed through the Helmholtz coil. Sparks were generated as shown in Figure 61. Nevertheless, the coil was not damaged.

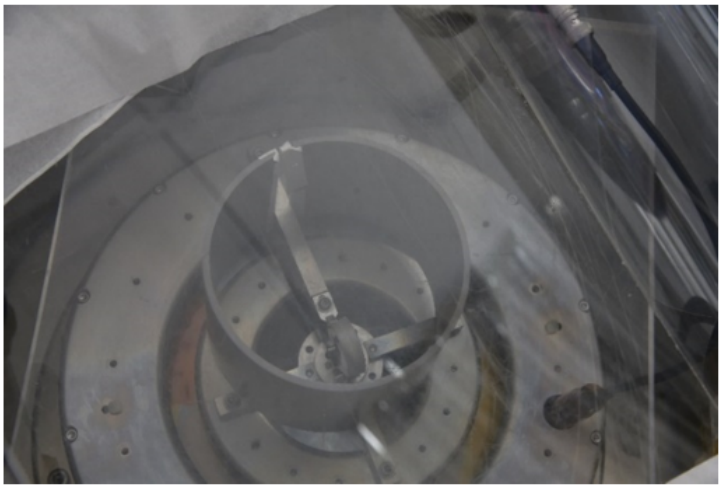

Figure 60: The prevention of damaging the chamber.

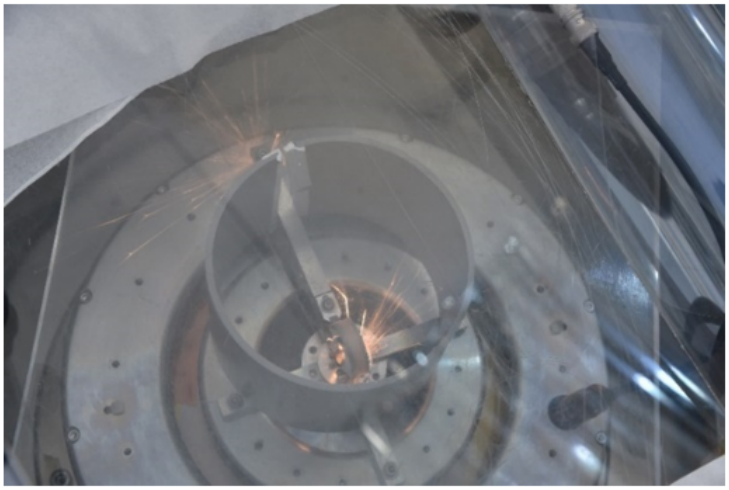

Figure 61: The discharge during the experiment.

During experiments, we measured the voltage of the capacitors in the system with the high-voltage probe (Tektronic-P6015A), and the current of the system with Rogowski coil, respectively. Figure 62 shows the signals of the capacitor's voltage in red and the current trace in blue in one of experiments. Except the high-frequency noise occurred at the beginning of the discharge, the current trace was an underdamped RLC oscillation. Unfortunately, the measured current trace was abnormal sometimes as shown Figure 63. The reason we suspected was that an arc discharge between the Rogowski coil and the coaxial transmission line occurred. We have solved the problem. The solution of the problem was given in Chapter 2.

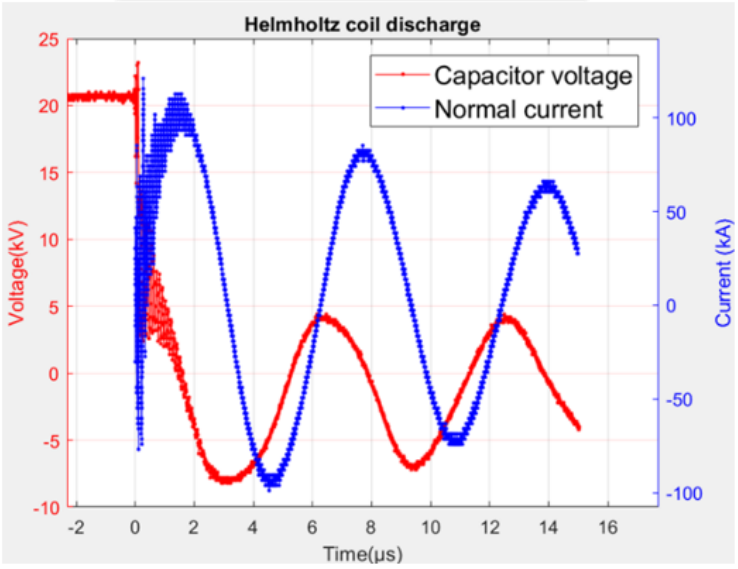

Figure 62: The capacitor's voltage and current trace.

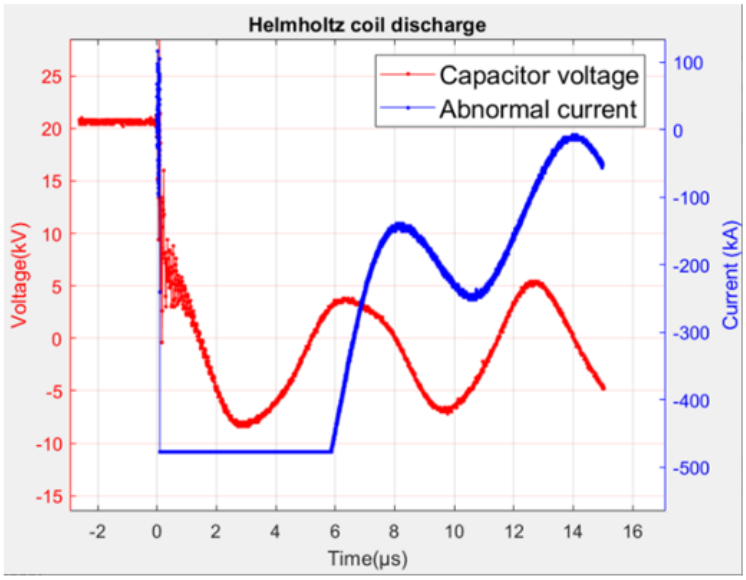

Figure 63: The capacitor's voltage and abnormal current trace of the system.

5.2 Discharge under low vacuum

In our project, the plasma plume needs to be generated and preheated first because the theta pinch only compresses a conductor. In other words, plasma needs to be generated prior to the theta-pinch. However, the system of the plasma plume is not completed yet. We tried to directly ionize the argon gas and pinch the plasma at the same time through the electric field generated by the pulsed magnetic field provided by the Helmholtz coil.

From previous experiments of Helmholtz coil discharged under atmospheric pressure, we knew that sparks were generated during the discharge. To reduce the impact of sparks on the experiment, we put some Kapton tape around the Helmholtz coil where there might be arcing. Finally, we closed the vacuum chamber and took the top-view images of the Helmholtz coil discharge using the newly installed raspberry-pi camera [21].

To keep the chamber under low vacuum, we injected a steady stream of argon gas into the chamber using a mass flow controller (KD-1000 1 CH) as shown in Figure 64. The flow rate was 5 standard cubic centimeter per minute (SCCM). On the other hand, only the rough pump was turned on. As a result, the pressure of argon in the chamber was around 0.5 torr. The reason we wanted to have chamber filled with argon with a pressure of 0.5 torr is in the following.

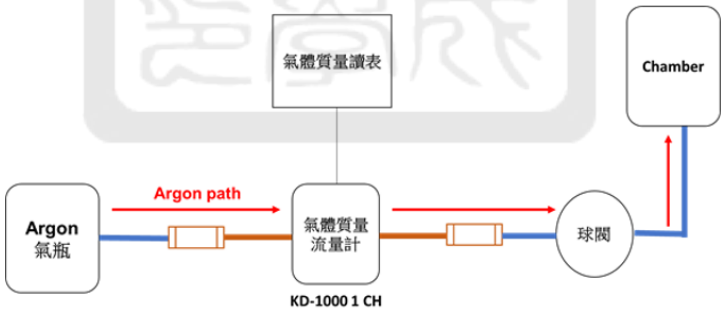

Figure 64: The path of argon gas flow in the system.

Firstly, we want to find out under what conditions argon gas can be ionized using the Paschen curve of argon gas. The Paschen curve is a curve that describes the required breakdown voltage V_B of an air gap with a given gap distance (d) and air pressure (P) as shown in Figure 65. Any voltages above the curve can cause a breakdown between the gap. We get the lowest breakdown voltage V_B required for ionization at the lowest point of the curve. Table 4 from the former student, Jun-Yu Chen, shows the lowest breakdown voltage V_B occurs at different products of the gap distance (d) and the air pressure (P) for Argon [22]. Then, we calculated the required

voltage that can be generated by the pulsed magnetic field from the Helmholtz coil.

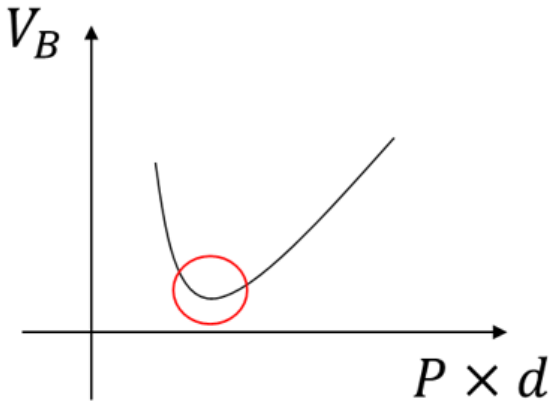

Figure 65: The schematic of the Paschen's curve.

Table 4: The data of breakdown voltage at the lower edge [22].

P × d(torr × mm)	V_B(V)
7.04	93
14.92	110
13.98	101
11.52	97
8.24	89
6.44	91
10.4	89
5.7	89
7.64	90
6.44	88

Assume that the magnetic field generated from the Helmholtz coil discharge is

$$B = B_0 \sin(\omega t) = 10 \sin(\omega t) \tag{19}$$

where $\omega = \frac{2\pi}{T} = 2\pi \times \frac{1}{1.6\mu s \times 4} = 9.8 \times 10^5$ rad/s using the period of the discharge current. $B_0 = 10$ is picked because it is the lowest magnetic field that will be generated as suggested in section 3.3. The induced voltage in the Helmholtz coil is

$$V = -\frac{d\phi}{dt} = -\pi r^2 \times [B_0 \omega \cos(\omega t)] = -\pi r^2 \times [10 \times (9.8 \times 10^5) \times \cos(\omega t)]. \tag{20}$$

Magnitudes of induced voltages of pseudo circles with different radii in space are shown in Figure 66 and Table 5.

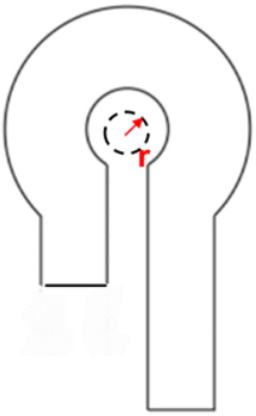

Figure 66: The pseudo circles with different radii inside the Helmholtz coil.

Table 5: The magnitude of induced voltage of pseudo circles at the different radius.

Radius, r(mm)	Induced voltage, V(volts)
1	$-31.0 \times \cos(\omega t)$
2	$-124.3 \times \cos(\omega t)$
3	$-279.8 \times \cos(\omega t)$
4	$-497.5 \times \cos(\omega t)$
5	$-777.3 \times \cos(\omega t)$

We defined the circumference of the pseudo circle in the Helmholtz coil as the gap of imaginated electrodes as shown in Figure 67 and Table 6. Furthermore, we assumed that the magnetic field generated from the Helmholtz coil is uniform in the space. Under the assumption, if the induced voltage is larger than the breakdown voltage at a specific pressure, the argon gas would be ionized becoming plasma.

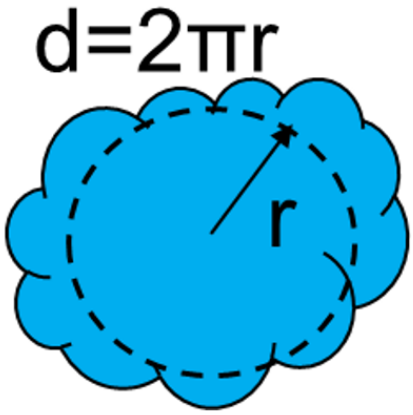

Figure 67: The schematic of the perimeter of the argon gas among the Helmholtz coil.

Table 6: The perimeter of the argon gas among the Helmholtz coil.

r(mm)	d(mm)
1	6.28
2	12.56
3	18.84
4	25.12
5	31.40

In Table 4, the breakdown voltage V_B=110 V when P×d is 14.92 (torr×mm) is the largest breakdown voltage. In other words, it is the hardest one to achieve. We use this number to estimate the required pressure. The estimated specific pressure is

$$P = \frac{14.92}{25.12} = 0.59 \text{ torr at r} = 4 \text{ mm}, \tag{21}$$

$$P = \frac{14.92}{31.4} = 0.47 \text{ torr at r} = 5 \text{ mm} \tag{22}$$

The estimated specific pressure is around 0.5 torr. Therefore, we kept our vacuum chamber at ∼0.5 torr.

Figure 68 is the side-view photo during the discharge. Unfortunately, the phenomenon of theta pinch did not occur in the experiment. In other words, the argon gas was not pre-ionized by the induced voltage. However, it was found that the glow discharge occurred in the chamber. We suspected the glow discharge occurred after the 1st peak of the current. The details are given in the next section. It should not contribute to the breakdown for theta pinch before the 1st peak of the current.

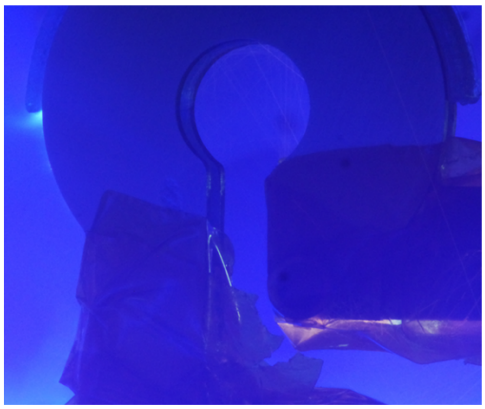

Figure 68: The side-view photo of the experiment.

5.3 Discharge under high vacuum

In this series of experiments, we did not inject argon gas into the chamber. However, we pumped the chamber down to 10^{-6} torr, which was in high vacuum regime. Similarly, we observed the glow discharge occurred in the chamber as shown in Figure 69. Fortunately, all current traces on the oscilloscope was normal as shown in Figure 70. Notice that the angular frequency of the current trace was $\omega = 1.01 \times 10^6$ and $\omega = 1.37 \times 10^6$ rad/s before and after $\sim$7 μs, respectively. We suspected that the inductance of system was changed at $\sim$7 μs, i.e., the current path was changed. In other words, the glow discharge in the chamber happened after 1.6 μs. Therefore, the glow discharge should not influence the theta pinch that will happen in the first quarter period.

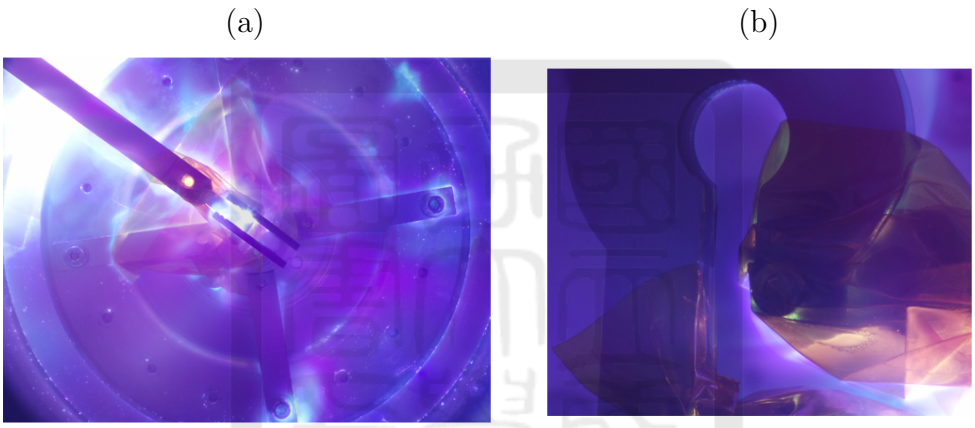

Figure 69: (a) The top-view photo in the experiment. (b) The side-view photo in the experiment.

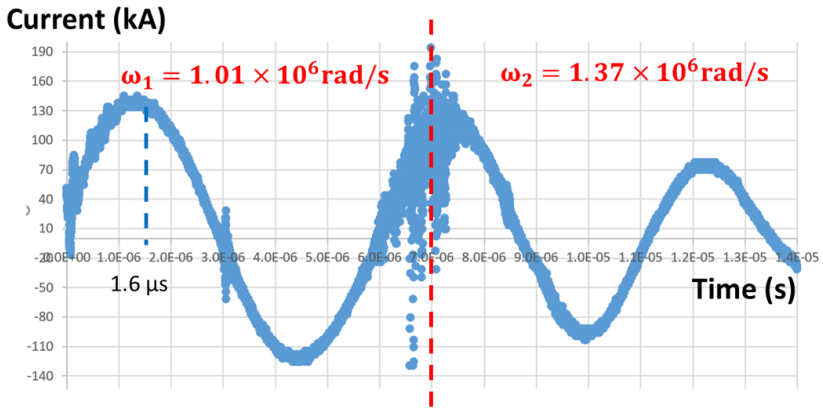

Figure 70: The one of the discharge currents measured with the Rogowski coil.

5.4 The magnetic field of the Helmholtz coil

After we conducted Helmholtz coil discharge tests under different conditions, we ensured that the Helmholtz coil can survive after the discharge. Then, we measured the magnetic field generated from the Helmholtz coil with B-dot probes in atmosphere. The magnetic field should not be influenced by the vacuum condition. However, it is much easier just to conduct experiments without operating vacuum system. In each experiment, we measured the magnetic fields at two locations at the same time. In Figure 71, the 3D printed support is used to hold two B-dot probes. One B-dot probe was placed at the center of Helmholtz coil while the other one was placed either 10 mm or 15 mm away from the Helmholtz coil center as shown in Figure 72.

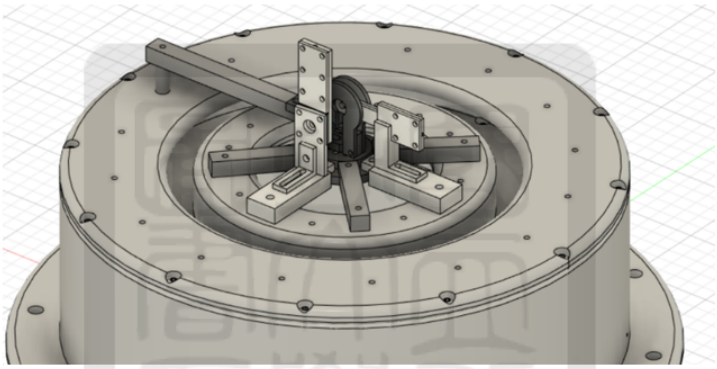

Figure 71: The two B-dot probe that placed near the Helmholtz coil.

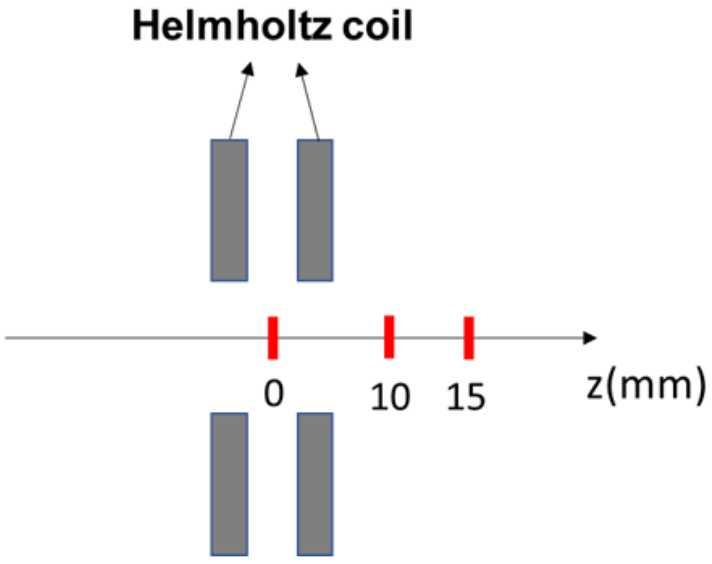

Figure 72: The location we measured with the B-dot probes.

5.4.1 The magnetic field at center of the Helmholtz coil

First of all, we measured the induced voltage V_{ind} of B-dot probe at the center of Helmholtz coil and 10 mm away from the coil on 2022/4/30. Figure 73 shows the result of one of Helmholtz coil discharge tests. Notice that the RC integrators of the B-dot probes were not used. We found the peak current (red curve) of the result was much larger than the peak current when the load was four AWG16 wires. It indicates that the inductance of the Helmholtz coil is much less than that of four AWG16 wires. The peak of the pulsed current was ∼140 kA. The blue curve is the $V_{ind,\,center}$ of the B-dot probe at the center of the Helmholtz coil while the green curve is the $V_{ind,\,10\,mm}$ of the B-dot probe at 10 mm away from the coil center. The two V_{ind} are proportional to the derivative of the current of the pulsed-power system.

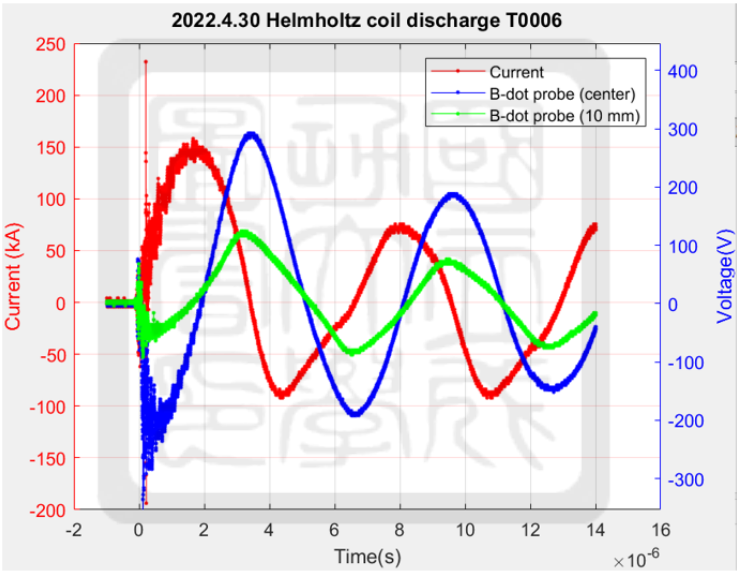

Figure 73: The raw data of the current and the two induced voltage.

According to equation (9), $B_{avg} = -\,C_{calib} \int V_{ind} dt = -41500 \pm 300 \int V_{ind} dt$. Therefore, we integrated the induced voltage. Numerically,

$$\int V_{ind} dt = \Delta t \sum_{i=1}^{n} V_{ind}(i) \;\text{ where } \Delta t = 10\,ns. \tag{23}$$

Finally, we got the relationship between $-\int V_{ind} dt$ of different locations versus time from two induced voltages. Figure 74 shows the result of $-\int V_{ind,\,center} dt$ versus time. Figure 75 shows the result of $-\int V_{ind,\,10\,mm} dt$ versus time. The trace of $-\int V_{ind,\,center} dt$ in Figure 74 behaves as an underdamped oscillation while the trace of $-\int V_{ind,\,10\,mm} dt$ in Figure 75 does not behave

like an underdamped oscillation. It looks like the B-dot probe 10 mm away from the coil center was collecting charges. Therefore, we only focus the result of $-\int V_{ind,\,center}dt$ in Figure 74. In order to estimate the magnetic field, we multiplied $-\int V_{ind,\,center}dt$ by $C_{calib} = 41500$. Figure 76 shows the relationship between $-\int V_{ind,\,center}dt$ and $B_{center}(t)$. According to the result, the Helmholtz coil can provide a pulsed magnetic field with the peak magnetic field of 11.4±1.0 T at the center. We are more interested in the first quarter period of the current trace since we expect the theta pinch occurs during the time. Gyroradius at peak magnetic field of a charged particle is

$$r = \frac{\sqrt{2mT}}{qB} \tag{24}$$

where m is the mass, T is the temperature, and q is the charge of the charged particle. Table 7 shows the gyroradius of different particles at 30 eV. Gyroradius of all particles are much less than the coil indicating that they will be confined.

Table 7: The gyroradius of the different particles.

	30 eV e^-	30 eV Ar^+	30 eV Xe^+
r(m)	1.1×10^{-6}	3×10^{-4}	5×10^{-4}

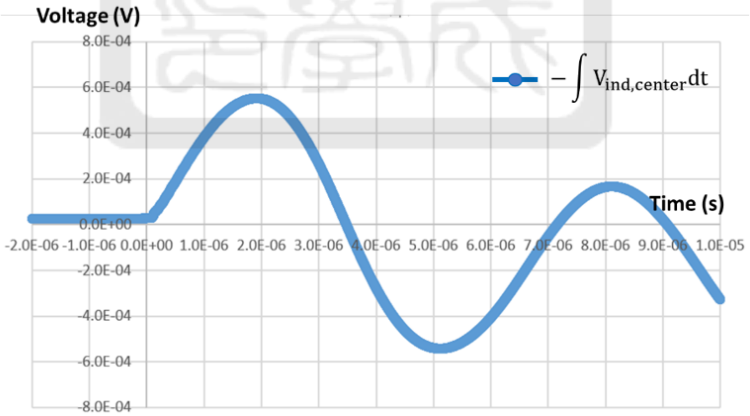

Figure 74: The result of $-\int V_{ind,\,center}dt$ versus time.

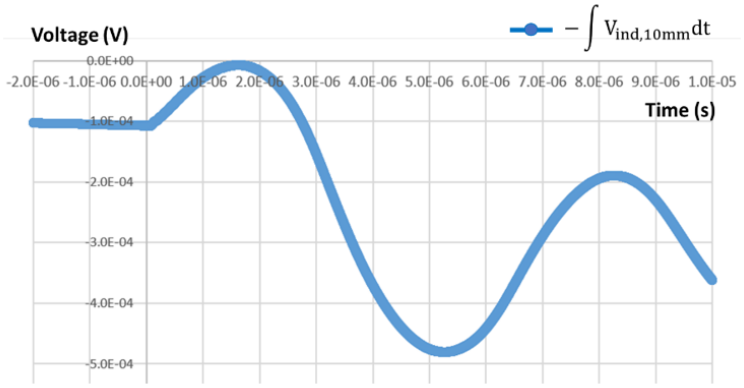

Figure 75: The result of $-\int V_{ind,\,10\,mm}dt$ versus time.

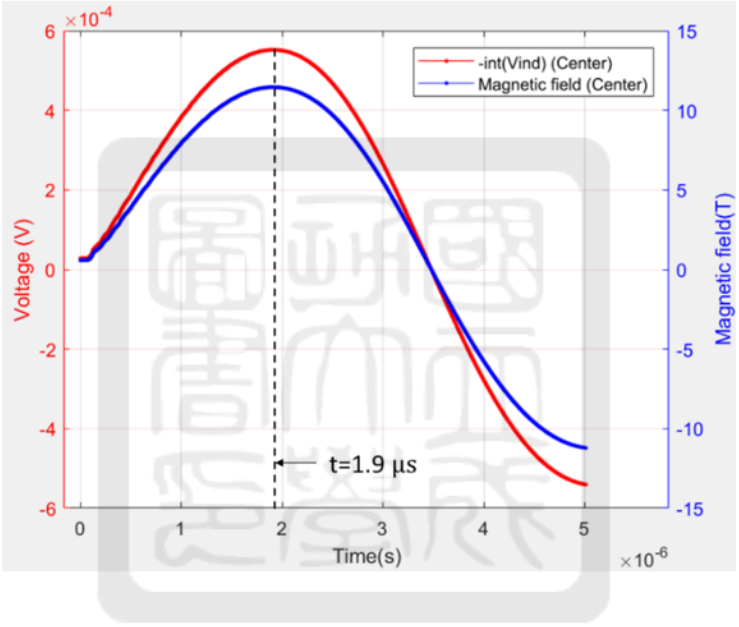

Figure 76: The relationship between $-\int V_{ind,\,center}dt$ and $B_{center}(t)$.

5.4.2 The magnetic field at 10 mm away from the Helmholtz coil center

In Helmholtz coil discharge on 2022/6/12, we integrated two B-dot probes with two RC integrators. Similarly, we placed two B-dot probes at the center of Helmholtz coil and at 10 mm away from the coil center. With RC integrators, we don't need to integrate the data numerically. Figure 77 shows one of experimental results. The phase of signal of B-dot probe at 10 mm away from the coil matched the phase of the current trace. However, the signal of B-dot probe at the center of coil was abnormal. Therefore, we only estimated the result of the signal of B-dot probe at 10 mm away from the coil. In Figure 78, the peak current in red is 170±8 kA and the Helmholtz coil generated a pulsed magnetic field with a peak magnetic field of 7±2 T.

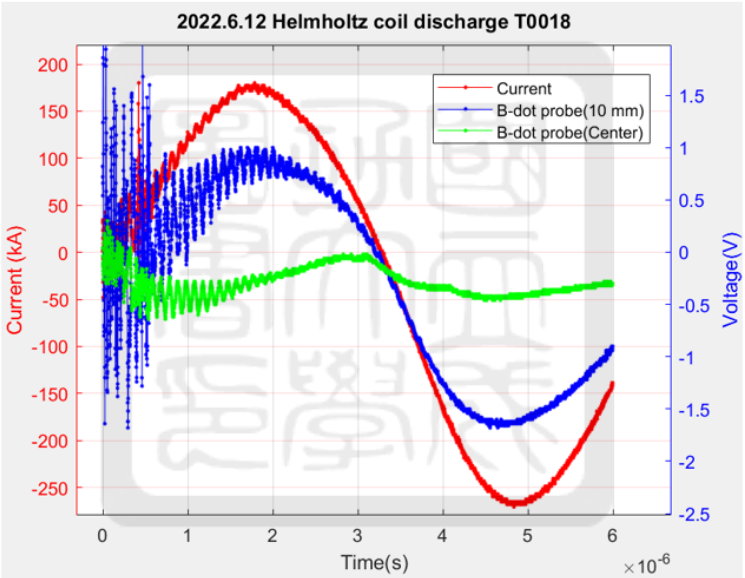

Figure 77: The raw data of one of 2022/6/12 Helmholtz coil discharge experiments.

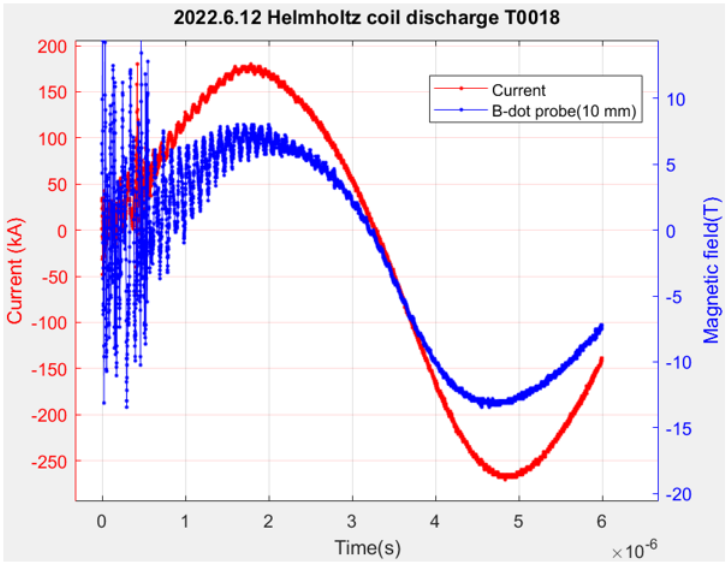

Figure 78: The current trace and the magnetic field in 10 mm.

5.4.3 The magnetic field at 15 mm away from the Helmholtz coil

In Helmholtz coil discharge on 2022/6/27, we placed two B-dot probes at the center of the Helmholtz coil and at 15 mm away from the coil center. Figure 79 shows one of experimental results. Unfortunately, the signals of B-dot probe at the center of coil were always abnormal. Therefore, we only estimated the result of the signal of B-dot probe at 15 mm away from the coil center. In Figure 80, the peak current in red was 200±5 kA and the Helmholtz coil generated a pulsed magnetic field with a peak magnetic field of 10±1 T.

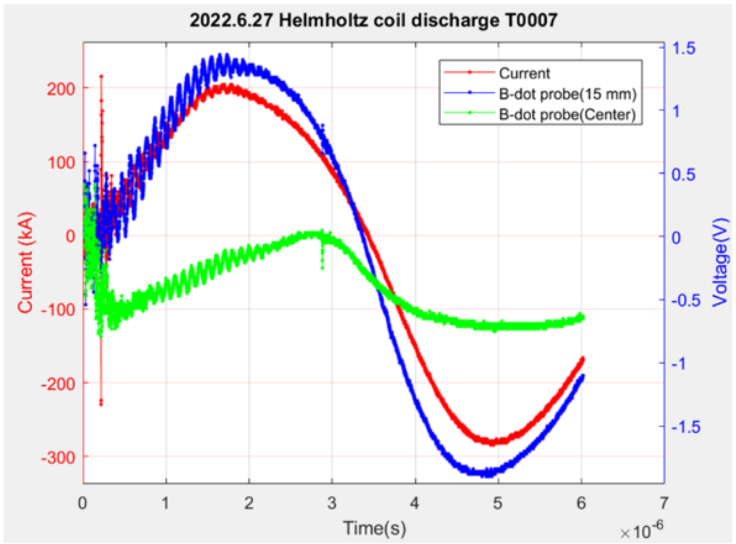

Figure 79: The raw data of one of 2022/6/27 Helmholtz coil discharge experiments.

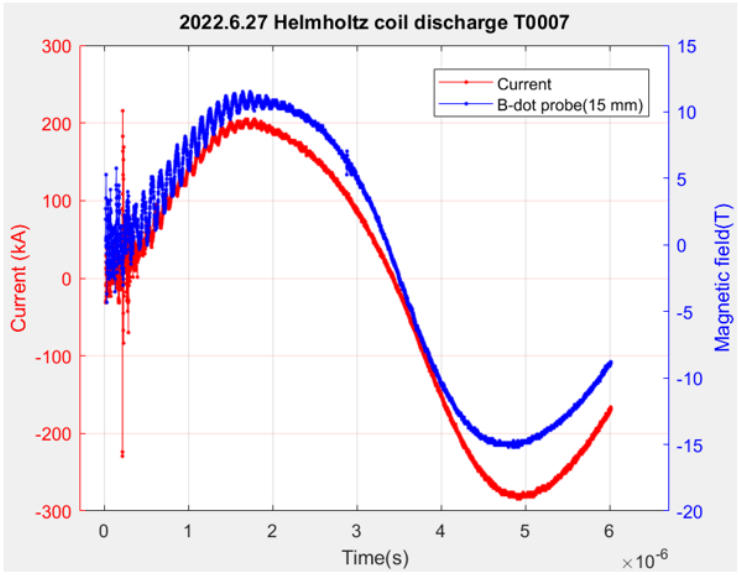

Figure 80: The current trace and the magnetic field in 15 mm.

5.5 Summary

In experiments, we tested the Helmholtz coil and saw if it can survive after the discharge. We have tested the discharge under three conditions: atmosphere, low vacuum, and high vacuum regime. After experiments, we knew that the Helmholtz coil was strong enough. In the condition of low vacuum, we tried to directly ionize the argon gas and pinch the plasma at the same time through the electric field generated by the pulsed magnetic field provided by the Helmholtz coil. However, the phenomenon of theta pinch was not observed in the experiment. In the condition of low vacuum and high vacuum, the glow discharge occurred in the chamber. We suspected the glow discharge should not influence the theta pinch that suppose to happen in the first quarter period. Then, we measured the magnetic fields generated from the Helmholtz coil. The peak magnetic fields of the Helmholtz coil at different locations are summarized in Table 8. Figure 81 shows the distribution of the magnetic field of the Helmholtz coil divided by the peak current. The blue curve represents the simulated magnetic field while the red data represents the measured magnetic field in experiments. The measured magnetic fields at center of coil and 10 mm away from coil matched the simulated magnetic field.

Table 8: The magnetic field at the different location.

Location (mm)	Magnetic field (T)	Peak current (A)
0 (center)	11.4 ± 1.0	150
10	7 ± 2	170
15	10 ± 1	200

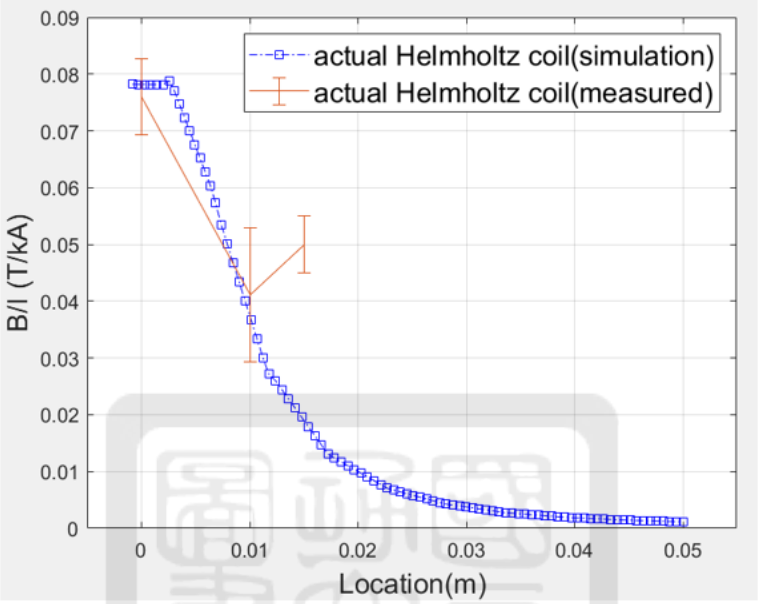

Figure 81: The normalized magnetic field distribution of the Helmholtz coil.

6 Future works

Following is the list of future works:

1. Generate a plasma plume: before generating a plasma plume, we need to build a gas-puff generator to provide an argon gas jet. Then, the plasma plume generator using arc discharge will be built. In Figure 82, the plasma plume generator consists of a pair of ring electrodes made by brass parallel to each other, a cylindrical insulator between two electrodes, and a small pulsed-power system with a 1-μF capacitor. When the gas jet propagates through two electrodes, the plasma plume will be generated and preheated by the arc discharge between two electrodes.

2. Theta pinch: when the plasma plume arrives the center of the Helmholtz coil, it will be compressed by a theta pinch driven by the pulsed-power system. We expect that the EUV light will be generated from the hot plasma with a temperature of ~30 eV. In experiments, we will integrate the plasma plume with the Helmholtz coil. Then, we will study the implosion of the theta pinch. Finally, we will measure characteristics of the radiation.

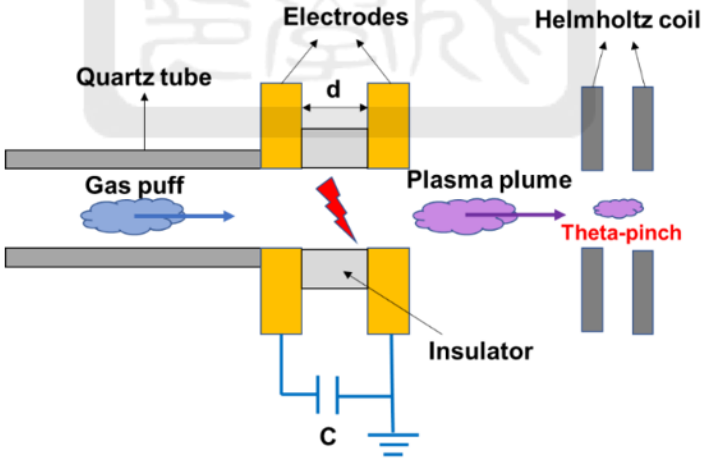

Figure 82: The schematic of the project for generating a plasma plume.

7 Summary

The goal of the work in this thesis is to use a Helmholtz coil to generate the magnetic field required for the theta pinch. We would like to heat the plasma via compression heating using a theta pinch. When the temperature of the plasma reaches about 30 eV, the plasma radiates EUV light.

A Q-switch laser (Q-smart 850-2w SLM) was integrated this year. It was used to take time-resolved images of plasma. Therefore, a new optical trigger-pulse generator was used to synchronize all signals between the laser and pulsed-power system. In experiments, the time difference between the flashlamp and the Q-switch was $\sim$400 μs so that it provides a proper intensity.

In order to drive the theta pinch, we used a pulsed-power system in the laboratory, which can provide a high current with a peak current of 100 $\sim$ 200 kA and a rise time of $\sim$ 1.6 μs. We measured the current of the pulsed-power system with a home-made Rogowski coil. However, the discharge current signal was often abnormal in the Helmholtz coil discharge test. The reason we suspected was the arcing between the Rogowski coil output connector and the top plate of the CTL. After putting more insulation using heat shrink tube and Kapton tape, the arcing problem was solved. We recalibrated the Rogowski coil with a Pearson monitor. The new calibration ratio was 137.4$\pm$0.4 kA/V with a time delay of 136$\pm$1 ns.

According to the theoretical formula, the ideal Helmholtz coil can generate a magnetic field in the range of 4.6 to 11.6 T at the center. In the simulation, thr current is uniformly distributed in the cross section. The Helmholtz coil can produce a magnetic field of 10.1 T at the center. Finally, we measured the magnetic field in discharge test. In order to measure the magnetic field of the Helmholtz coil, we built the B-dot probe. The B-dot probe was a single-turn coil which was made of 0.5-mm enameled copper wires. The diameter of the B-dot probes was 5 mm. Before we measured the magnetic field of the Helmholtz coil, the B-dot probe was calibrated by an known magnetic field provided by a solenoid. The magnetic field generated from the solenoid was $B = (3.00 \pm 0.05) \cdot I + (0.96 \pm 0.05)$ [G]. Afterward, a pulsed current flowing through the solenoid for generating a pulsed magnetic field inside the solenoid was used to calibrate the B-dot probe. By comparing the induced voltage of the B-dot probe and the magnetic field of the solenoid, we obtained the conversion ratio C_{calib} in equation (9). The conversion ratio C_{calib}

was 41500±300 (T/V·sec). Additionally, we made two RC integrators for integrating induced voltage of B-dot probes. We obtained the measured magnetic field from the B-dot probe with the RC integrators directly and got $B_{measured}(T)=(8.0\pm0.1)\times V_B$ (V).

After Helmholtz coil discharge tests, we knew that the Helmholtz coil was strong enough to survive after the discharge. In the condition of low vacuum, we tried to directly ionize the argon gas and pinch the plasma at the same time through the electric field generated by the pulsed magnetic field provided by the Helmholtz coil. However, the phenomenon of theta pinch was not observed in the experiment. In the condition of low vacuum and high vacuum, the glow discharge occurred in the chamber. We suspected the glow discharge should not influence the theta pinch happening in the first quarter period. Then, we measured the magnetic fields generated by the Helmholtz coil. The magnetic field at the center of the Helmholtz coil was 11.4±1.0 T. Then, we integrated two B-dot probes with two RC integrators. In Helmholtz coil discharge on 2022/6/12, Helmholtz coil generated a pulsed magnetic field with a peak magnetic field of 7±2 T at 10 mm away from the Helmholtz coil. In Helmholtz coil discharge on 2022/6/27, Helmholtz coil generated a pulsed magnetic field with a peak magnetic field of 10±1 T at 15 mm away from the Helmholtz coil.

8 Reference

[1]http://www.semiconductorchiller.com/manufacturing-of-semiconductor/

[2]https://en.wikipedia.org/wiki/Moore%27s_law

[3]https://case.ntu.edu.tw/blog/?p=33519

[4]https://finance.technews.tw/2019/01/25/euv-asml-2018/

[5]F.A.Ebrahim1, W. H. Gaber1, M. E. Abdel-kader1. Estimation of the Current Sheath Dynamics and Magnetic Field for Theta Pinch by Snow Plow Model Simulation.

[6]http://capst.ncku.edu.tw/PGS/index.php/pulsed-power-generator/

[7]https://en.wikipedia.org/wiki/Helmholtz_coil

[8]V.Borisov, A. Eltzov, A. Ivanov, O. Khristoforov, Yu. Kirykhin, A. Vinokhodov, V. Vodchits, V. Mishhenko, and A. Prokofiev. Discharge produced plasma source for EUV lithography.

[9]https://aip.scitation.org/doi/full/10.1063/5.0079450

[10]http://capst.ncku.edu.tw/PGS/index.php/pulsed-power-generator/

[11]Jia-Kai Liu. Study of the gas puff in the EUV light source using a theta pinch. Master thesis. National Cheng Kung University Institute of Space and Plasma Sciences, 2022.

[12]https://aip.scitation.org/doi/full/10.1063/5.0079450

[13]https://www.quantel-laser.com/en/products/item/q-smart-850-mj-.html

[14]Po-Yu Chang,1, ∗ Yen-Cheng Lin,1 Ming-Hsiang Kuo,1. One-kilojoule Pulsed-Power Generator for Imploding Conical-Wire Arrays.

[15]Ming-Hsiang Kuo. Study the plasma disk generated from the head-on collisions of two plasma jets. Master thesis. National Cheng Kung University Institute of Space and Plasma Sciences, 2022.

[16]https://www.comsol.com/comsol-multiphysics

[17]I.H.HUTCHINSON. Principles of Plasma Diagnostics Second edition. Massachusetts Institute of Technology.

[18]Sayak Bose, Manjit Kaur, Kshitish K. Barada, Joydeep Ghosh, Prabal K. Chattopadhyay and Rabindranath Pal. Understanding the working of a B-dot probe.

[19]https://en.wikipedia.org/wiki/Twisted_pair.

[20]https://file.yzimgs.com/365081/2011050521414051.pdf. WT10A 數字特斯拉計

[21]Ming-Hsiang Kuo. Study the plasma disk generated from the head-on collisions of two plasma jets. Master thesis. National Cheng Kung University Institute of Space and Plasma Sciences, 2022.

[22]Jun-Yun Cheng. 109 Annual Report.

9 Appendix

A.1 The code of the new optical trigger-pulse generator

```
* Pin definition:
 *                    output: 8 - TLED - trigger indicator
 *                            7 - SLED - standby indicator
 *                              6 - LaserLED - Laser synchronization
indicator
 *                    input: 12 - FGS - (10 Hz) Function generator input
 *                            2 - triggerpin - trigger switch (push button)
 *                              4 - standbypin - standy switch (toggle
switch)
 *                            3 - laserpin - laser synchronization switch
(toggle switch)

int TLED = 8;
int SLED = 7;
int LaserLED = 6; // by Po-Yu, pin for the syncrhonization status LED
int FGS =12; // by Po-Yu, Cheng-Han's code
int triggerpin = 2;
int standbypin = 4;
int laserpin = 3; // by Po-Yu, pin to read the synchronization status of with
the laser.
int t0 = 0;
int s0 = 0;
```

```
int t1 = 0;
int s1 = 1;
int t2;
int s2;
int st;
int tt;
bool b1;   // by Po-Yu, buffer1 of storing the signal of the function generator.
bool b2;   // by Po-Yu, buffer2 of storing the signal of the function generator.
int laserstatus;   // by Po-Yu, status of the synchronization with laser. 0-without laser; 1-with laser.
int triggerflag; // by Po-Yu, status of triggering
int ittriger; // by Po-Yu, a counter to prevent that the status stuck at the firing mode

void setup()
{
  pinMode(TLED, OUTPUT);
  pinMode(SLED, OUTPUT);
  pinMode(LaserLED, OUTPUT);   // by Po-Yu, laser synchronization indicator
  pinMode(triggerpin, INPUT);
  pinMode(standbypin, INPUT);
```

```
  pinMode(FGS, INPUT); // by Po-Yu, read the signal from the function
generator
  pinMode(laserpin, INPUT);
  Serial.begin(9600);
}

void loop()
{
 t2 = digitalRead(triggerpin);
 s2 = digitalRead(standbypin);
 laserstatus = digitalRead(laserpin);    // by Po-Yu, read the laser
synchronization status.
 digitalWrite(LaserLED,laserstatus);    // by Po-Yu, indicate the laser
synchronization status.
 st = s2-s1;
 tt = t2-t1;
 if (s0==0)
 {
  if(st==1)
  {
    s0 = 1;
    s1 = s2;
    digitalWrite(SLED,s0);
  }
```

```
  else
  {
     s1 = s2;
  }
 }
 else
 {
  if (st==-1)
  {
     s0=0;
     digitalWrite(SLED,s0);
     s1 = s2;
  }
  else if (tt==1)
  {
     t0=1;
     if (laserstatus==0) //by Po-Yu, output the trigger pulse WITHOUT
synchronization.
     {
        digitalWrite(TLED,t0);
        delayMicroseconds(1250);
        digitalWrite(TLED,0);
     }
     else //by Po-Yu, output the trigger pulse WITH synchronization.
```

```
{
  triggerflag = 1;
  ittriger = -30000;
  while (triggerflag ==1 && ittriger < 30000 )    //the loop will stop
after 10000 iteration to prevent being stuck in the loop
  {
    boolean b1 =digitalRead(FGS);
    if(b1 == LOW)
    {
      boolean b2 =digitalRead(FGS);
      if(b2 == HIGH)
      {
        //delay 99 ms in total,
        delay(99);
        digitalWrite(TLED,HIGH);
        delayMicroseconds(1250);
        digitalWrite(TLED,LOW);
        triggerflag = 0;
      }
      ittriger = ittriger + 1;
    }
  }
}
t1 = t2;
```

```
        s0 = 0;
        digitalWrite(SLED,s0);
    }
    else
    {
        t1 = t2;
    }
  }
}
```

A.2 The CAD drawing of the Helmholtz coil

1. Helmholtz coil_ coil

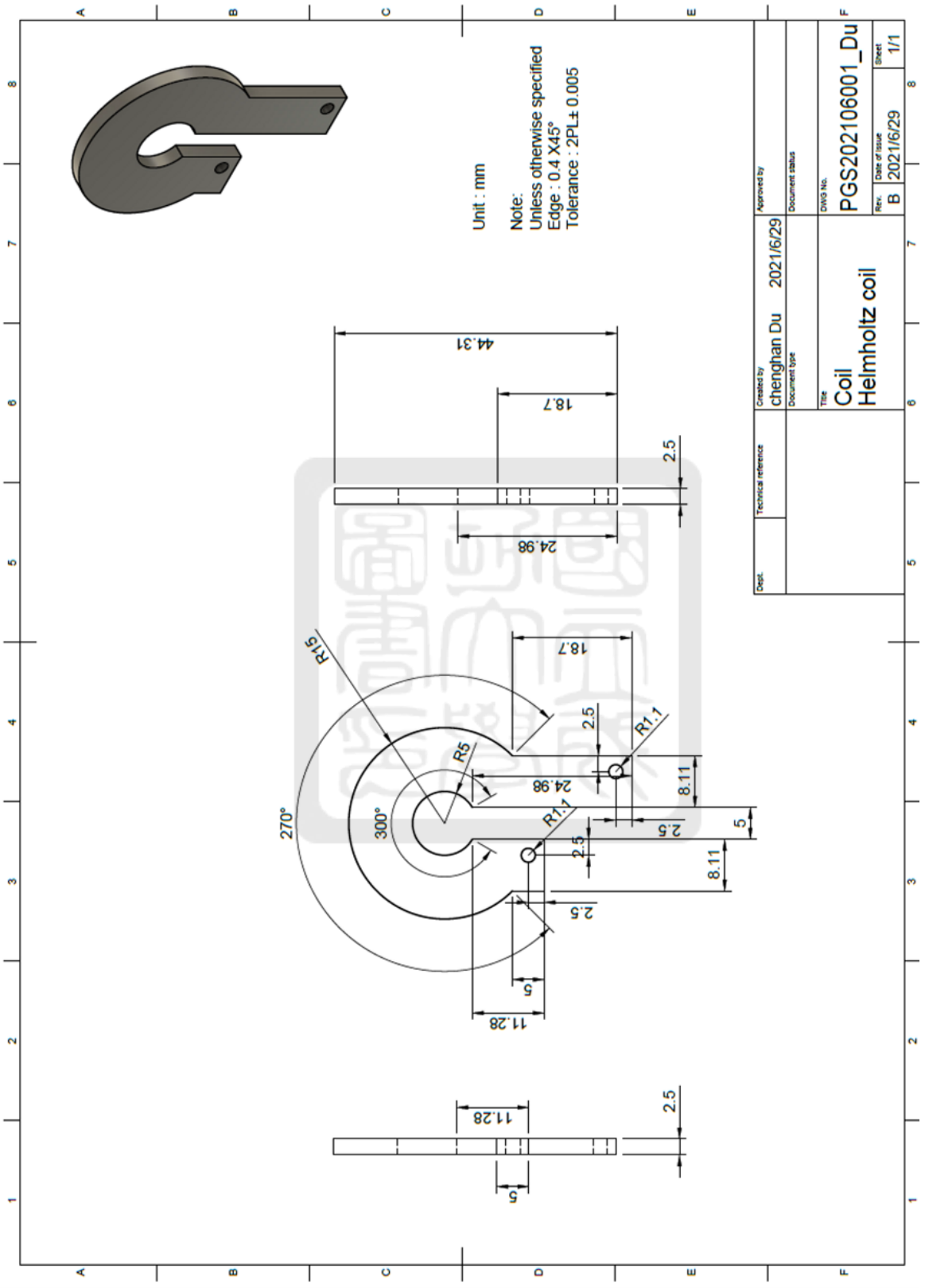

2. Helmholtz coil_ Helmholtz coil horizontal holder

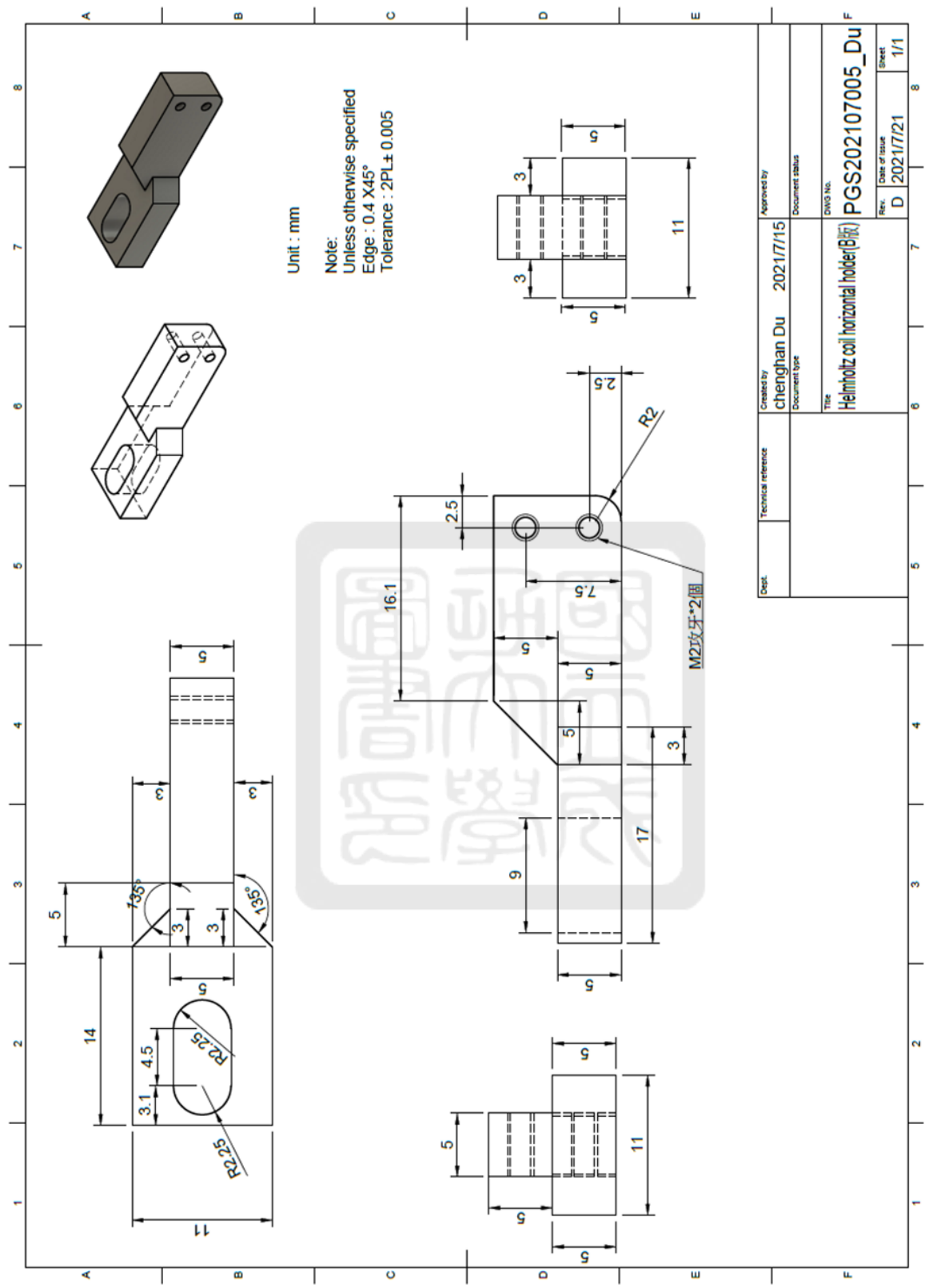

3. Helmholtz coil_ bottom coil connector

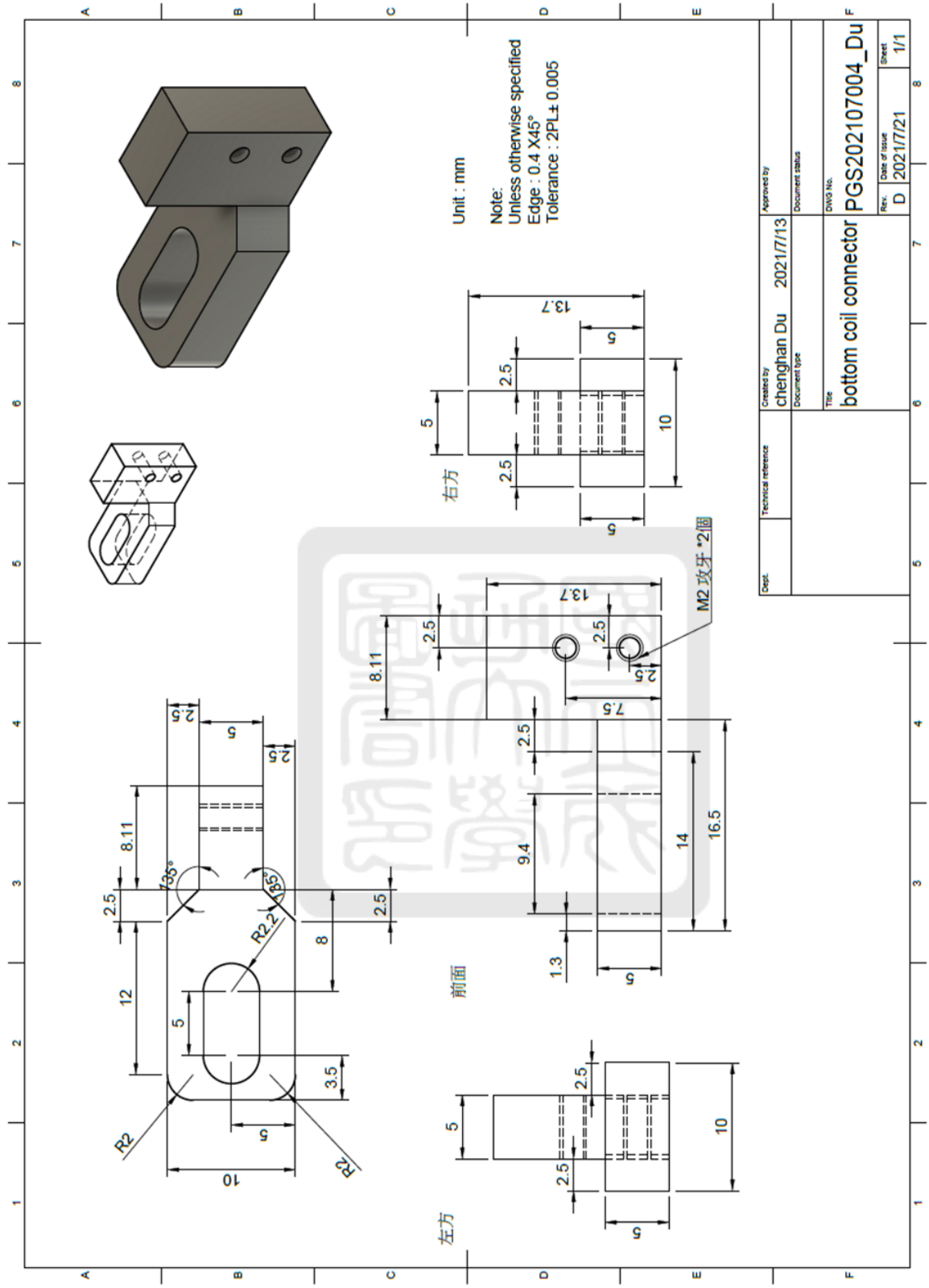

4. The new bottom wire support

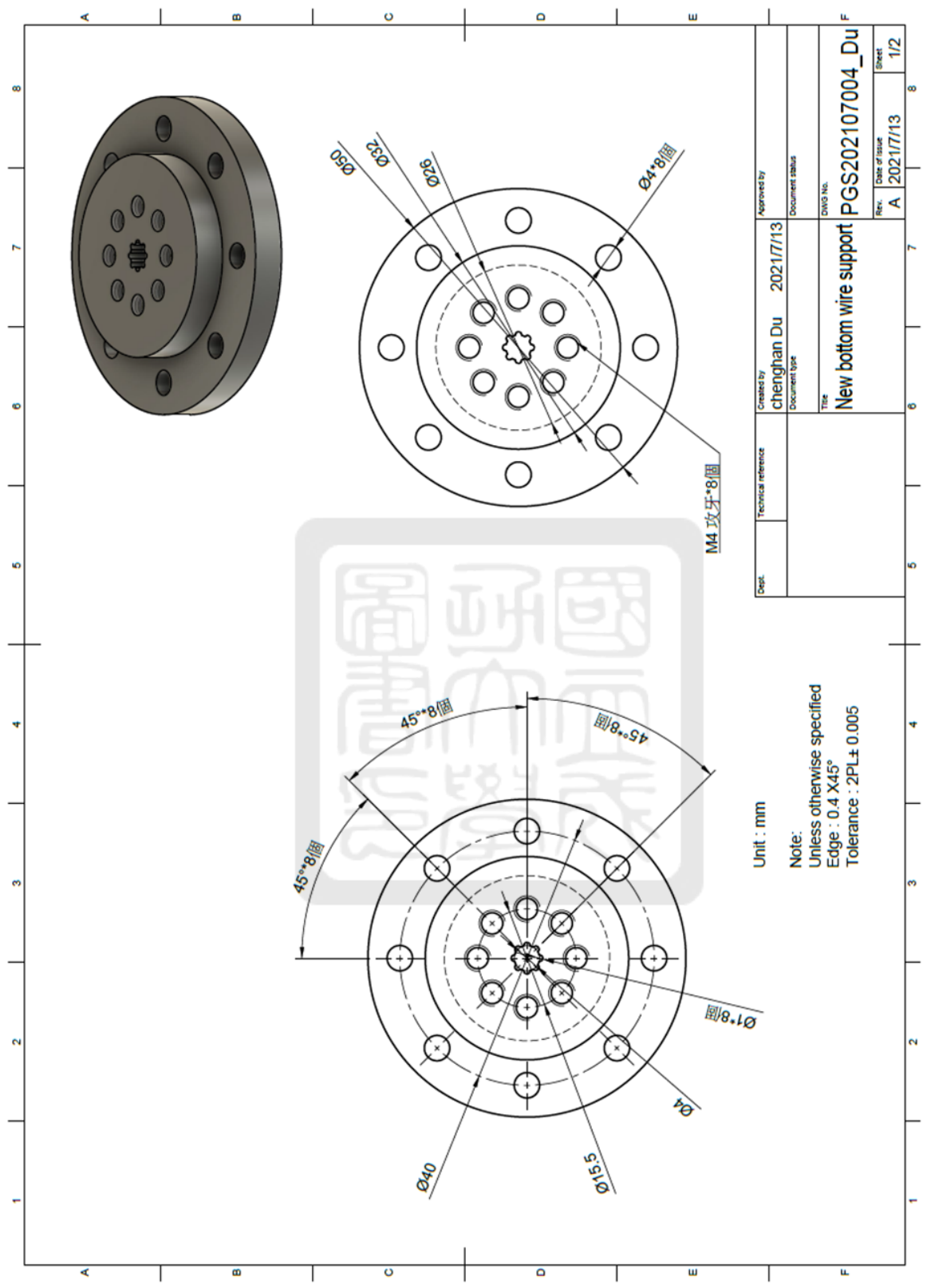

A.3 The CAD drawing of the plastic spacer

- The plastic spacer

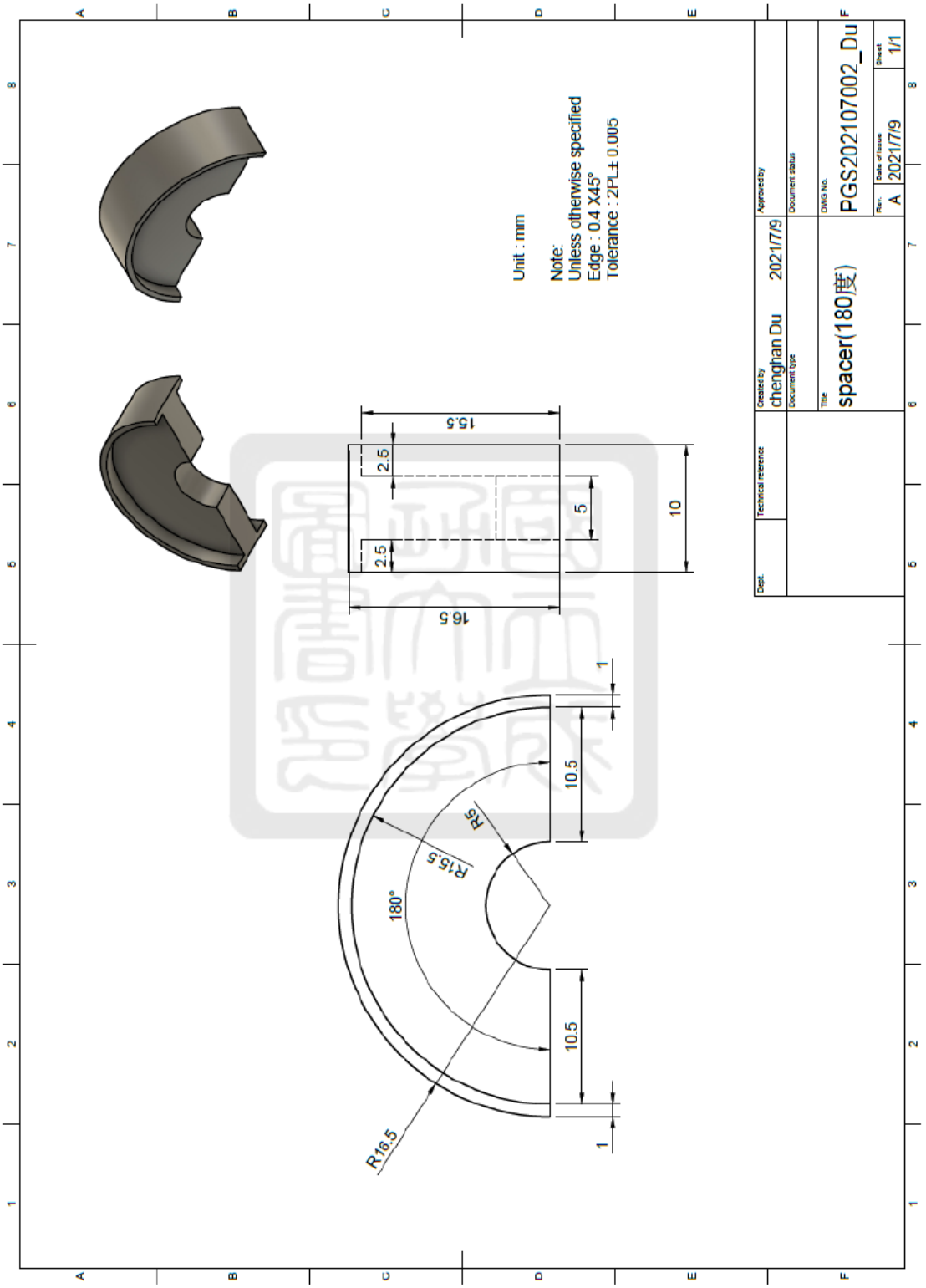

A.4 The CAD drawing of the support of the Gauss meter probe

- The support of the Gauss meter probe

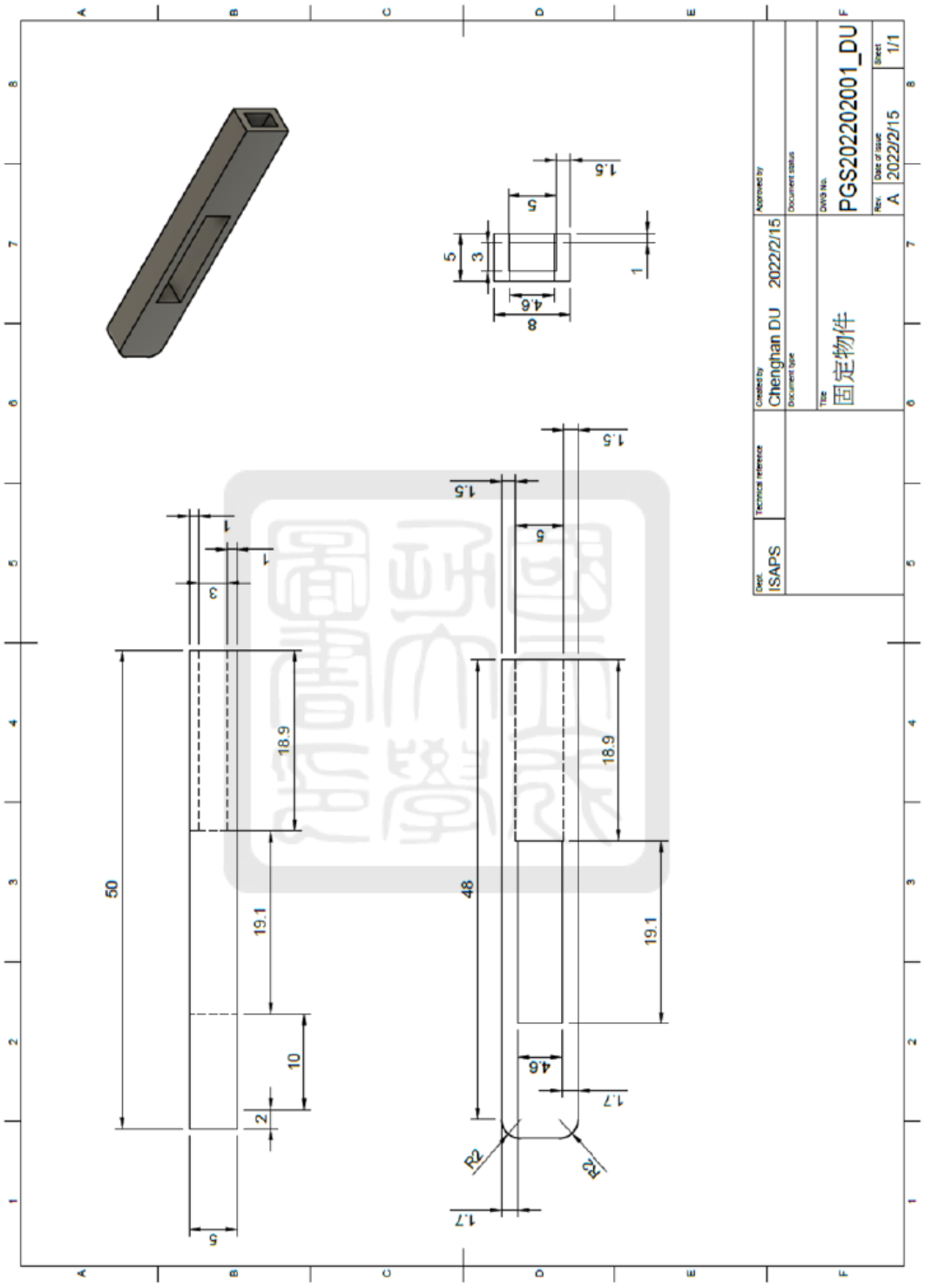

A.4 The venders of all components

Component	Vender	Location
Helmholtz coil(不鏽鋼)	Helmholtz coil(不鏽鋼)	台南市南區明興路619巷345號
Stand of optical table (塑鋼)	威正塑膠有限公司	台南市仁德區忠義路662號
雷射警示燈(壓克力板)	長明壓克力行	台南市東區崇善東路37號
鋁材	金全通鋁材有限公司	台南市歸仁區和順路一段296號
電饋通	東昕實業有限公司	台南市永康區中正南路220巷39號
電子零件	南一電子有限公司	台南市中西區民族路二段95號

A.5 Folder of data

- The experimental data is located in /Experiments/2020_cdu in the lab drive.
- The CAD drawing is located in /Drawing/chenghan in the lab drive.